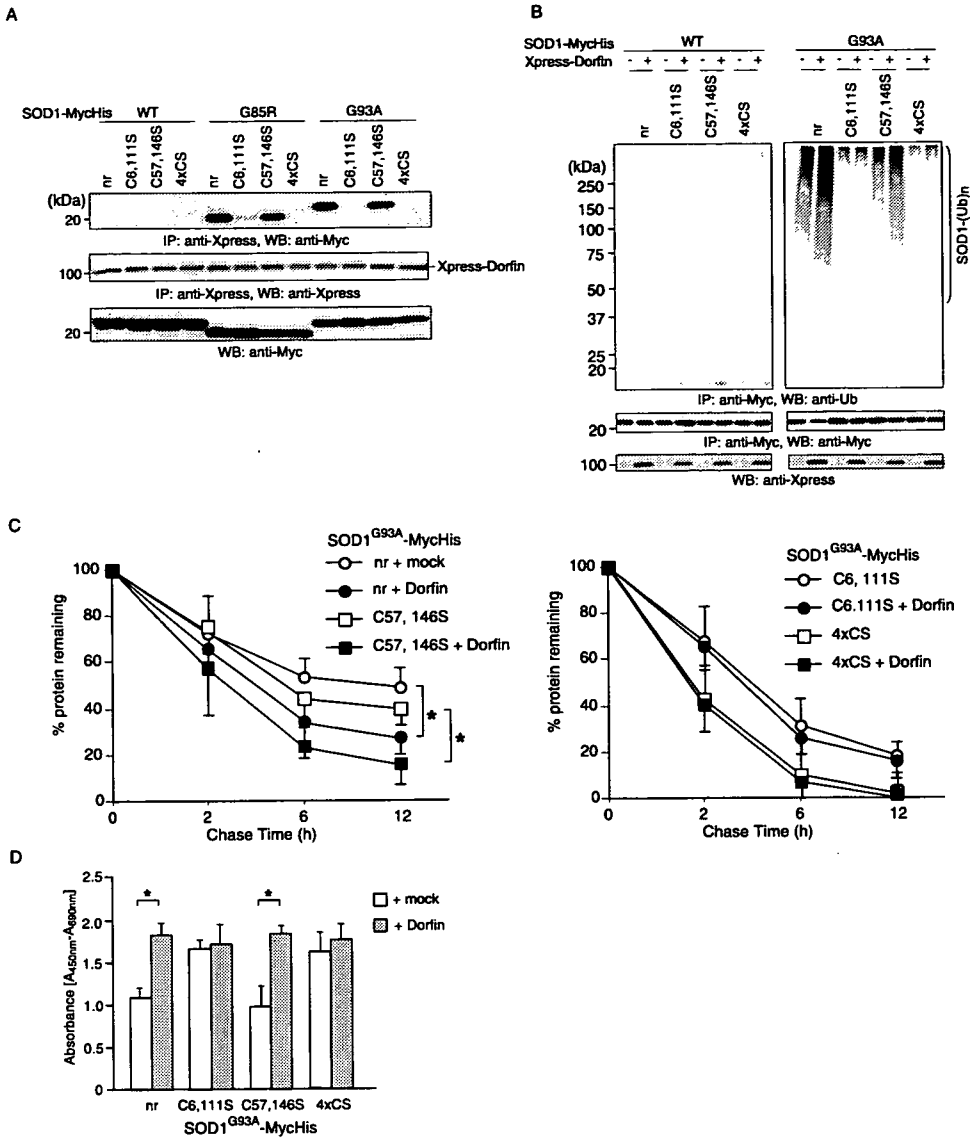

FIGURE 7. **Ubiquityl ligase Dorfin binds, ubiquitylates, and promotes degradation of disulfide-linked mutant SOD1.** *A*, replacement of Cys^6 and Cys^{111} nearly eliminated the interaction of Dorfin with mutant SOD1. Various SOD1-MycHis were co-transfected with Xpress-Dorfin. After immunoprecipitation with anti-Xpress antibody, the resulting precipitates and cell lysates were analyzed by Western blotting with anti-Myc antibody. *B, in vivo*, Dorfin failed to promote ubiquitylation of mutant SOD1 with the Cys^6 and Cys^{111} replacement. Western blotting of SOD1-Myc-His immunoprecipitates with anti-ubiquitin antibody. *C*, Dorfin failed to promote degradation of mutant SOD1 with both Cys^6 and Cys^{111} replaced. Cycloheximide chase analysis of G93A mutant SOD1 with Cys^6 and Cys^{111}-replacements (*left panel*) or with Cys^{57} and Cys^{146}-replacements (*right panel*) in the presence or absence of overexpressed Xpress-Dorfin. *D*, Dorfin prevented neurotoxicity by mutant SOD1 with intact Cys^6 and Cys^{111} residues. Cell viability was measured by the WST-1-based assay. Data are mean ± S.D. values of three independent experiments. Statistical analyses were carried out by unpaired *t* test. *, $p < 0.01$. *nr*, SOD1 without replacement in cysteine residue; *4×CS*, all four cysteines replaced by serines.

111 and with a G86R mutation corresponding to G85R mutation in human SOD1, degeneration of motor neurons in the spinal cord has been observed (40). These results imply that, if one of either the Cys^6 or Cys^{111} residues is present, it can still be a disease-causing SOD1. Our data here also revealed that replacement of only one of the Cys residues at positions 6 or 111 had modest effects on the formation of aggregates (Fig. 2).

Cytoplasmic proteins are degraded mainly via two pathways, the ubiquitin-proteasome pathway (6) and via autophagy (7). Previous studies have shown that mutant SOD1 proteins are turned over more rapidly than wild-type SOD1 (12, 18, 19). Two distinct ubiquitin ligases, Dorfin and NEDL1, were reported to specifically ubiquitylate mutant but not wild-type SOD1 (20, 21). These studies suggest that mutant SOD1 is degraded by the ubiquitin-proteasome pathway and that the accelerated turnover of mutant SOD1 is mediated in part by this pathway. Impairment of the proteasome activities may contribute to ALS pathogenesis (28, 41, 42). We showed here that proteasome inhibition led to a dose-dependent accumulation of aberrant disulfide-linked high molecular weight mutant SOD1 (Fig. 1), suggesting that disulfide-linking mediates ubiquitylation of mutant SOD1. In fact, we found that Dorfin ubiquitylated mutant SOD1 by recognizing the Cys^6 and Cys^{111} disulfide cross-linked form and targeted it for proteasomal degradation (Fig. 7). Mutant SOD1, in which the Cys^6 and Cys^{111} were replaced, was not ubiquitylated (Fig. 3), and its rate of degradation was not affected in the presence of Dorfin (Fig. 7). It is possible that mutant SOD1 lacking Cys^6 and Cys^{111} may be degraded directly by the proteasome without ubiquitylation (43) or by autophagy (44), but further studies are needed to address this issue.

The appearance of mutant SOD1 aggregates in motor neurons of familial ALS patients and mouse models has suggested that aggregation plays an important role in neurotoxicity (31). However, conflicting results have been reported on the correlation between aggregate formation and cell death. One report showed that aggregate formation of mutant $SOD1^{A4V}$ and $SOD1^{V148G}$ does not correlate with cell death (45), whereas another study using live cell-imaging techniques reported that the ability of mutant $SOD1^{G85R}$ and $SOD1^{G93A}$ proteins to form aggregates directly correlates with neuronal cell death (46). These controversies also exist in other neurodegenerative diseases (47, 48). In this study, we clearly showed a direct link among intermolecular disulfide bond-mediated high molecular weight complex formation, visible aggregate formation, and neurotoxicity (Figs. 2–4).

Furukawa *et al.* (16) reported that formation of disulfide-linked multimers need not involve the non-conserved Cys residues, Cys^6 and Cys^{111}, and that the conserved Cys residues, Cys^{57} and Cys^{146}, play an important role in the apo-form of

SOD1 multimerization upon oxidative stress. Our results underscore the importance of Cys^{6} and Cys^{111} for high molecular weight aggregate formation, ubiquitylation, and neurotoxicity in Neuro-2a cells. This discrepancy may result from differences in experimental conditions; we studied human SOD1 proteins expressed in Neuro-2a cells, and Furukawa *et al.* used the purified apo-form of human SOD1 from *Escherichia coli.* Further studies will clarify the roles of each of the Cys residues of the mutant SOD1 protein in the ALS pathogenesis *in vivo* by generating transgenic mice bearing mutant SOD1 lacking Cys^{6} and Cys^{111} or Cys^{57} and Cys^{146}.

REFERENCES

1. McCord, J. M., and Fridovich, I. (1969) *J. Biol. Chem.* **244,** 6049–6055
2. Fridovich, I. (1974) *Adv. Enzymol. Relat. Areas. Mol. Biol.* **41,** 35–97
3. Rosen, D. R. (1993) *Nature* **364,** 362
4. Valentine, J. S., Doucette, P. A., and Potter, S. Z. (2005) *Annu. Rev. Biochem.* **74,** 563–593
5. Crapo, J. D., Oury, T., Rabouille, C., Slot, J. W., and Chang, L. Y. (1992) *Proc. Natl. Acad. Sci. U. S. A.* **89,** 10405–10409
6. Fridovich, I. (1986) *Adv. Enzymol. Relat. Areas. Mol. Biol.* **58,** 61–97
7. Fisher, C. L., Cabelli, D. E., Tainer, J. A., Hallewell, R. A., and Getzoff, E. D. (1994) *Proteins* **19,** 24–34
8. Arnesano, F., Banci, L., Bertini, I., Martinelli, M., Furukawa, Y., and O'Halloran, T. V. (2004) *J. Biol. Chem.* **279,** 47998–48003
9. Freedman, R. B. (1995) *Curr. Opin. Struct. Biol.* **5,** 85–91
10. Lindenau, J., Noack, H., Possel, H., Asayama, K., and Wolf, G. (2000) *Glia* **29,** 25–34
11. Tiwari, A., and Hayward, L. J. (2003) *J. Biol. Chem.* **278,** 5984–5992
12. Borchelt, D. R., Lee, M. K., Slunt, H. S., Guarnieri, M., Xu, Z. S., Wong, P. C., Brown, R. H., Jr., Price, D. L., Sisodia, S. S., and Cleveland, D. W. (1994) *Proc. Natl. Acad. Sci. U. S. A.* **91,** 8292–8296
13. Ratovitski, T., Corson, L. B., Strain, J., Wong, P., Cleveland, D. W., Culotta, V. C., and Borchelt, D. R. (1999) *Hum. Mol. Genet* **8,** 1451–1460
14. Rakhit, R., Crow, J. P., Lepock, J. R., Kondejewski, L. H., Cashman, N. R., and Chakrabartty, A. (2004) *J. Biol. Chem.* **279,** 15499–15504
15. Doucette, P. A., Whitson, L. J., Cao, X., Schirf, V., Demeler, B., Valentine, J. S., Hansen, J. C., and Hart, P. J. (2004) *J. Biol. Chem.* **279,** 54558–54566
16. Furukawa, Y., and O'Halloran, T. V. (2005) *J. Biol. Chem.* **280,** 17266–17274
17. Furukawa, Y., Fu, R., Deng, H. X., Siddique, T., and O'Halloran, T. V. (2006) *Proc. Natl. Acad. Sci. U. S. A.* **103,** 7148–7153
18. Hoffman, E. K., Wilcox, H. M., Scott, R. W., and Siman, R. (1996) *J. Neurol. Sci.* **139,** 15–20
19. Johnston, J. A., Dalton, M. J., Gurney, M. E., and Kopito, R. R. (2000) *Proc. Natl. Acad. Sci. U. S. A.* **97,** 12571–12576
20. Niwa, J., Ishigaki, S., Hishikawa, N., Yamamoto, M., Doyu, M., Murata, S., Tanaka, K., Taniguchi, N., and Sobue, G. (2002) *J. Biol. Chem.* **277,** 36793–36798
21. Miyazaki, K., Fujita, T., Ozaki, T., Kato, C., Kurose, Y., Sakamoto, M., Kato, S., Goto, T., Itoyama, Y., Aoki, M., and Nakagawara, A. (2004) *J. Biol. Chem.* **279,** 11327–11335
22. Niwa, J., Ishigaki, S., Doyu, M., Suzuki, T., Tanaka, K., and Sobue, G. (2001) *Biochem. Biophys. Res. Commun.* **281,** 706–713
23. Marin, I., and Ferrus, A. (2002) *Mol. Biol. Evol.* **19,** 2039–2050
24. Lee, H. J., and Lee, S. J. (2002) *J. Biol. Chem.* **277,** 48976–48983
25. Scherzinger, E., Lurz, R., Turmaine, M., Mangiarini, L., Hollenbach, B., Hasenbank, R., Bates, G. P., Davies, S. W., Lehrach, H., and Wanker, E. E. (1997) *Cell* **90,** 549–558
26. Bailey, C. K., Andriola, I. F., Kampinga, H. H., and Merry, D. E. (2002) *Hum. Mol. Genet.* **11,** 515–523
27. Wang, J., Xu, G., and Borchelt, D. R. (2002) *Neurobiol. Dis.* **9,** 139–148
28. Urushitani, M., Kurisu, J., Tsukita, K., and Takahashi, R. (2002) *J. Neurochem.* **83,** 1030–1042
29. Gurney, M. E., Pu, H., Chiu, A. Y., Dal Canto, M. C., Polchow, C. Y., Alexander, D. D., Caliendo, J., Hentati, A., Kwon, Y. W., Deng, H. X., Chen, W., Zhai, P., Sufit, R. L., and Siddique, T. (1994) *Science* **264,** 1772–1775
30. Bruijn, L. I., Houseweart, M. K., Kato, S., Anderson, K. L., Anderson, S. D., Ohama, E., Reaume, A. G., Scott, R. W., and Cleveland, D. W. (1998) *Science* **281,** 1851–1854
31. Cleveland, D. W., and Rothstein, J. D. (2001) *Nat. Rev. Neurosci.* **2,** 806–819
32. Watanabe, M., Dykes-Hoberg, M., Culotta, V. C., Price, D. L., Wong, P. C., and Rothstein, J. D. (2001) *Neurobiol. Dis.* **8,** 933–941
33. Wang, J., Xu, G., and Borchelt, D. R. (2006) *J. Neurochem.* **96,** 1277–1288
34. Jonsson, P. A., Graffmo, K. S., Andersen, P. M., Brannstrom, T., Lindberg, M., Oliveberg, M., and Marklund, S. L. (2006) *Brain* **129,** 451–464
35. Deng, H. X., Shi, Y., Furukawa, Y., Zhai, H., Fu, R., Liu, E., Gorrie, G. H., Khan, M. S., Hung, W. Y., Bigio, E. H., Lukas, T., Dal Canto, M. C., O'Halloran, T. V., and Siddique, T. (2006) *Proc. Natl. Acad. Sci. U. S. A.* **103,** 7142–7147
36. Getzoff, E. D., Tainer, J. A., Stempien, M. M., Bell, G. I., and Hallewell, R. A. (1989) *Proteins* **5,** 322–336
37. Briggs, R. G., and Fee, J. A. (1978) *Biochim. Biophys. Acta* **537,** 86–99
38. McRee, D. E., Redford, S. M., Getzoff, E. D., Lepock, J. R., Hallewell, R. A., and Tainer, J. A. (1990) *J. Biol. Chem.* **265,** 14234–14241
39. Lepock, J. R., Frey, H. E., and Hallewell, R. A. (1990) *J. Biol. Chem.* **265,** 21612–21618
40. Ripps, M. E., Huntley, G. W., Hof, P. R., Morrison, J. H., and Gordon, J. W. (1995) *Proc. Natl. Acad. Sci. U. S. A.* **92,** 689–693
41. Kabashi, E., Agar, J. N., Taylor, D. M., Minotti, S., and Durham, H. D. (2004) *J. Neurochem.* **89,** 1325–1335
42. Cheroni, C., Peviani, M., Cascio, P., Debiasi, S., Monti, C., and Bendotti, C. (2005) *Neurobiol. Dis.* **18,** 509–522
43. Di Noto, L., Whitson, L. J., Cao, X., Hart, P. J., and Levine, R. L. (2005) *J. Biol. Chem.* **280,** 39907–39913
44. Kabuta, T., Suzuki, Y., and Wada, K. (2006) *J. Biol. Chem.* **281,** 30524–30533
45. Lee, J. P., Gerin, C., Bindokas, V. P., Miller, R., Ghadge, G., and Roos, R. P. (2002) *J. Neurochem.* **82,** 1229–1238
46. Matsumoto, G., Stojanovic, A., Holmberg, C. I., Kim, S., and Morimoto, R. I. (2005) *J. Cell Biol.* **171,** 75–85
47. Arrasate, M., Mitra, S., Schweitzer, E. S., Segal, M. R., and Finkbeiner, S. (2004) *Nature* **431,** 805–810
48. Saudou, F., Finkbeiner, S., Devys, D., and Greenberg, M. E. (1998) *Cell* **95,** 55–66

Neurobiology of Disease

Reversible Disruption of Dynactin 1-Mediated Retrograde Axonal Transport in Polyglutamine-Induced Motor Neuron Degeneration

Masahisa Katsuno, Hiroaki Adachi, Makoto Minamiyama, Masahiro Waza, Keisuke Tokui, Haruhiko Banno, Keisuke Suzuki, Yu Onoda, Fumiaki Tanaka, Manabu Doyu, and Gen Sobue

Department of Neurology, Nagoya University Graduate School of Medicine, Showa-ku, Nagoya 466-8550, Japan

Spinal and bulbar muscular atrophy (SBMA) is a hereditary neurodegenerative disease caused by an expansion of a trinucleotide CAG repeat encoding the polyglutamine tract in the *androgen receptor* (*AR*) gene. To elucidate the pathogenesis of polyglutamine-mediated motor neuron dysfunction, we investigated histopathological and biological alterations in a transgenic mouse model of SBMA carrying human pathogenic AR. In affected mice, neurofilaments and synaptophysin accumulated at the distal motor axon. A similar intramuscular accumulation of neurofilament was detected in the skeletal muscle of SBMA patients. Fluoro-gold labeling and sciatic nerve ligation demonstrated an impaired retrograde axonal transport in the transgenic mice. The mRNA level of dynactin 1, an axon motor for retrograde transport, was significantly reduced in the SBMA mice resulting from pathogenic AR-induced transcriptional dysregulation. These pathological events were observed before the onset of neurological symptoms, but were reversed by castration, which prevents nuclear accumulation of pathogenic AR. Overexpression of dynactin 1 mitigated neuronal toxicity of the pathogenic AR in a cell culture model of SBMA. These observations indicate that polyglutamine-dependent transcriptional dysregulation of dynactin 1 plays a crucial role in the reversible neuronal dysfunction in the early stage of SBMA.

Key words: polyglutamine; spinal and bulbar muscular atrophy; androgen; neurofilament; axonal transport; retrograde; dynactin

Introduction

Spinal and bulbar muscular atrophy (SBMA), or Kennedy's disease, is a hereditary neurodegenerative disease resulting from a loss of bulbar and spinal motor neurons (Kennedy et al., 1968; Sobue et al., 1989). Patients present with muscle atrophy and weakness of proximal limbs associated with bulbar palsy, tongue atrophy and contraction fasciculation (Katsuno et al., 2006). The disease affects exclusively adult males, whereas females carrying the mutant *androgen receptor* (*AR*) are seldom symptomatic (Schmidt et al., 2002). The molecular basis of SBMA is an expansion of a trinucleotide CAG repeat, which encodes the polyglutamine tract in the first exon of the *AR* gene (La Spada et al., 1991). This type of mutation has also been found to cause a variety of neurodegenerative disorders, termed polyglutamine diseases, such as Huntington's disease (HD), several forms of spinocerebellar ataxia, and dentatorubral pallidoluysian atrophy (Gatchel and Zoghbi, 2005). Although expression of the causative gene in each of these diseases is ubiquitous, selective neuronal cell death is observed in disease-specific areas of the CNS, suggesting a common molecular basis for these polyglutamine diseases.

Nuclear accumulation of pathogenic protein containing elongated polyglutamine is a crucial step in the pathophysiology of these diseases, providing an important therapeutic target (Adachi et al., 2005; Banno et al., 2006). The aberrant polyglutamine protein has a propensity to form aggregates in the nucleus and inhibits the function of transcriptional factors and coactivators, resulting in transcriptional perturbation (Cha, 2000; Gatchel and Zoghbi, 2005). In support of this hypothesis, altered expression of a variety of genes has been demonstrated in transgenic mouse models of polyglutamine diseases (Sugars and Rubinsztein, 2003). Although polyglutamine-induced transcriptional dysregulation is likely to be central to the pathogenesis of polyglutamine diseases, it has yet to be elucidated which genes are responsible for the selective neurodegeneration (Gatchel and Zoghbi, 2005).

No treatments have been established for polyglutamine diseases, but the androgen blockade therapy, surgical or medical castration, has shown striking therapeutic effects in the SBMA transgenic mouse model (Katsuno et al., 2002, 2003; Chevalier-Larsen et al., 2004). Androgen deprivation strongly inhibits the ligand-dependent nuclear accumulation of pathogenic AR protein, resulting in a striking improvement in neurological and histopathological findings of male mice.

In the present study, we investigated the molecular pathophysiology of motor neuron dysfunction in a transgenic mouse

Received July 18, 2006; revised Sept. 21, 2006; accepted Oct. 6, 2006.

This work was supported by a Center of Excellence grant from the Ministry of Education, Culture, Sports, Science and Technology, Japan, and by grants from the Ministry of Health, Labor and Welfare, Japan. We have no financial conflict of interest that might be construed to influence the results or interpretation of this manuscript. We thank Jun-ichi Miyazaki for kindly providing the pCAGGS vector.

Correspondence should be addressed to Dr. Gen Sobue, Department of Neurology, Nagoya University Graduate School of Medicine, 65 Tsurumai-cho, Showa-ku, Nagoya 466-8550, Japan. E-mail: sobueg@med.nagoya-u.ac.jp.

DOI:10.1523/JNEUROSCI.3032-06.2006

 0270-6474/06/2612106-12$15.00/0

model of SBMA. Polyglutamine-induced transcriptional dysregulation of the dynactin p150 subunit (dynactin 1), an axonal motor-associated protein, resulted in perturbation of retrograde axonal transport in spinal motor neurons in the early stage of the disease. These processes were reversed by castration, which inhibits nuclear accumulation of pathogenic AR. A defect in axonal trafficking of neurofilaments and synaptic vesicles, the potential molecular basis for the reversible pathogenesis, appears to contribute to the initiation of symptoms, and may account for the selective degeneration of motor neurons in SBMA.

Materials and Methods

Generation and maintenance of transgenic mouse. AR-24Q and AR-97Q mice were generated as described previously (Katsuno et al., 2002). Briefly, the full-length human *AR* fragment harboring 24 or 97 CAGs was subcloned into the *Hind*III site of the pCAGGS vector (Niwa et al., 1991) and microinjected into BDF1-fertilized eggs. Five founders with AR-97Q were obtained. These mouse lines were maintained by backcrossing them to C57BL/6J mice. All symptomatic lines (2–6, 4–6, and 7–8) were examined in the present study. All animal experiments were approved by the Animal Care Committee of the Nagoya University Graduate School of Medicine. Mice were given sterile water *ad libitum*. In the experiments where it was called for, sodium butyrate [a histone deacetylase (HDAC) inhibitor] was administered at a concentration of 4 g/L in distilled water from 5 weeks of age until the end of the analysis, as described previously (Minamiyama et al., 2004).

Neurological testing and castration after onset. Mice were subjected to the Rotarod task (Economex Rotarod; Colombus Instruments, Columbus, OH), and cage activity was measured (AB system; Neuroscience, Tokyo, Japan) as described previously (Katsuno et al., 2002). Gait stride was measured in 50 cm of footsteps, and the maximum value was recorded for each mouse. The onset of motor impairment was determined using weekly rotarod task analyses. Male AR-97Q mice were castrated or sham-operated via the abdominal route under ketamine–xylazine anesthesia (50 mg/kg ketamine and 10 mg/kg xylazine, i.p.) within 1 week after the onset of rotarod impairment.

Immunohistochemistry and immunofluorescent analysis. Ten-micrometer-thick sections were prepared from paraffin-embedded tissues, and immunohistochemistry was performed as described previously (Katsuno et al., 2002). Formalin-fixed tail samples were washed with 70% ethanol and decalcified with 7% formic acid–70% ethanol for 7 d before embedding in paraffin. Sections to be immunostained for dynactin 1, dynein intermediate chain, dynein heavy chain, and dynamitin were first microwaved for 20 min in 50 mM citrate buffer, pH 6.0. Sections to be immunostained for polyglutamine (1C2 antibody) were treated with formic acid for 5 min at room temperature. The following primary antibodies were used: anti-dynactin 1 (p150^{glued}, 1:250; BD Transduction, San Diego, CA), anti-dynein intermediate chain (1:500; Millipore, Temecula, CA), anti-dynein heavy chain (1:100; Sigma-Aldrich, St. Louis, MO), anti-dynamitin (1:1000; BD Transduction), anti-polyglutamine, 1C2 (1:10,000; Millipore), antiphosphorylated high molecular weight neurofilament (NF-H) (SMI31, 1:1000; Sternberger Monoclonals, Lutherville, MD), anti-nonphosphorylated NF-H (SMI32, 1:5000; Sternberger Monoclonals), and anti-synaptophysin (1:10,000; Dako, Glostrup, Denmark).

For immunofluorescent analysis of skeletal muscle, mice were deeply anesthetized with ketamine–xylazine and perfused with PBS followed by 4% paraformaldehyde fixative in phosphate buffer, pH 7.4. Gastrocnemius muscles were dissected free, frozen quickly by immersion in cooled acetone and powdered CO_2. Longitudinal, 30 μm, cryostat sections were placed on a silane-coated slide in a drop of 3% disodium EDTA, air dried at room temperature, and fixed in methanol/acetone (50:50 v/v). After blocking with PBS containing 5% goat serum and 1% BSA for 30 min at room temperature, sections were incubated with 5 μg/ml Oregon green-conjugated α-bungarotoxin (Invitrogen, Eugene, OR) for 60 min at room temperature. Sections were incubated with antiphosphorylated NF-H (SMI31, 1:5000; Sternberger Monoclonals), anti-synaptophysin (1:50,000; Dako), or anti-Rab3A (1:5000; BD Transduction) antibodies at 4°C overnight, and then with Alexa-546-conjugated goat anti-mouse IgG (1:1000; Invitrogen). Sections were examined with an IX71 inverted microscope (Olympus, Tokyo, Japan). For double staining of the skeletal muscle, paraffin-embedded sections were treated with TNB blocking buffer (PerkinElmer, Boston, MA) and incubated with anti-AR antibody (N-20, 1:500; Santa Cruz Biotechnology, Santa Cruz, CA) together with antiphospho-NF-H.

For immunostaining of human tissues, autopsy specimens of lumbar spinal cord and intercostal muscle obtained from a genetically diagnosed SBMA patient (78-year-old male) and those from a neurologically normal patient (75 years old) were used. The collection of tissues and their use for this study were approved by the Ethics Committee of Nagoya University Graduate School of Medicine. Spinal cord sections at 10 μm were incubated with anti-dynactin 1 antibody (p150^{glued}, 1:250; BD Transduction). Thirty-micrometer-thick cryostat sections of intercostal muscle were incubated with 150 μg/ml Alexa-488-conjugated α-bungarotoxin (Invitrogen) and then with antiphosphorylated NF-H (SMI31, 1:200; Sternberger Monoclonals).

Retrograde Fluoro-gold neurotracer labeling. For labeling neurons with intramuscular injection of tracer, mice were anesthetized with ketamine–xylazine, and a small incision was made in the skin of the left calf to expose the gastrocnemius muscle. A total volume of 4.5 μl of 2.5% Fluoro-gold solution (Biotium, Hayward, CA) in PBS was injected in three different parts of the muscle (proximal, middle, and distal) using a 10 μl Hamilton syringe. For labeling by the nerve stump method, the sciatic nerve was exposed and transected at mid-thigh level. A small polyethylene tube containing 2.5% Fluoro-gold solution was applied to the proximal stump of the cut sciatic nerve, and sealed with Vaseline to prevent leakage. Mice were anesthetized 44 h after Fluoro-gold administration with ketamine–xylazine and perfused with PBS followed by 4% paraformaldehyde in phosphate buffer, pH 7.4. Spinal cords were removed and postfixed with 4% paraformaldehyde in phosphate buffer for 2 h, floated in 10 and 15% sucrose for 4 h each and in 20% sucrose overnight. The samples were sectioned longitudinally on a cryostat at 30 μm and mounted on silane-coated slides. The number of Fluoro-gold labeled motor neurons was counted in serial spinal cord sections with an IX71 inverted microscope (Olympus) using a wide-band UV filter. Some specimens were immunostained for dynactin immediately after the number of Fluoro-gold-labeled motor neurons was counted.

Western blot analysis. SH-SY5Y cells were lysed in CellLytic lysis buffer (Sigma-Aldrich) containing a protease inhibitor mixture (Roche, Mannheim, Germany) 2 d after transfection. Mice were killed under ketamine–xylazine anesthesia. Their tissues were snap-frozen with powdered CO_2 in acetone and homogenized in 50 mM Tris, pH 8.0, 150 mM NaCl, 1% NP-40, 0.5% deoxycholate, 0.1% SDS, and 1 mM 2-mercaptoethanol containing 1 mM PMSF and 6 μg/ml aprotinine and then centrifuged at 2500 × *g* for 15 min at 4°C. The supernatant fractions were separated on 5–20% SDS-PAGE gels (10 μg protein for the nerve roots or 40 μg for the spinal cord, per lane) and then transferred to Hybond-P membranes (Amersham Pharmacia Biotech, Buckinghamshire, UK), using 25 mM Tris, 192 mM glycine, 0.1% SDS, and 10% methanol as transfer buffer. Immunoblotting was performed using the following primary antibodies: anti-dynactin 1 (p150^{glued}, 1:250; BD Transduction), anti-dynein intermediate chain (1:1000; Millipore), anti-dynein heavy chain (1:200; Sigma-Aldrich), anti-dynamitin (1:250; BD Transduction), anti-α-tubulin (1:5000; Sigma-Aldrich), antiphosphorylated NF-H (SMI31, 1:100,000; Sternberger Monoclonals), and anti-nonphosphorylated NF-H (SMI32, 1:1000; Sternberger Monoclonals). The immunoblots were digitalized (LAS-3000 imaging system; Fujifilm, Tokyo, Japan), signal intensities of three independent blots were quantified with Image Gauge software version 4.22 (Fujifilm), and the means ± SD were expressed in arbitrary units.

Ligation of mouse sciatic nerve. Under anesthesia with ketamine–xylazine, the skin of the right lower limb was incised. The right sciatic nerve was exposed and ligated at mid-thigh level using surgical thread. For immunofluorescent analysis, operated mice were decapitated under deep anesthesia with ketamine–xylazine 8 h after ligation and perfused with 4% paraformaldehyde fixative in phosphate buffer, pH 7.4. The right sciatic nerve segment, including at least 5 mm both proximal and distal to

the ligated site, was removed. The nonligated, left sciatic nerve was also taken out in the same manner as the right nerve. The removed nerves were placed into fixative for 4 h, transferred consecutively to 10, 15, and 20% sucrose in 0.01 M PBS, pH 7.4, for 4 h each at 4°C, mounted in Tissue-Tek OCT compound (Sakura, Tokyo, Japan), and frozen with powdered CO_2 in acetone. Ten-micrometer-thick cryostat sections were prepared from the frozen tissues, blocked with normal goat serum (1:20), incubated with anti-synaptophysin (1:50,000; Dako) at 4°C overnight, and then with Alexa-546-conjugated goat anti-mouse IgG (1:1000; Invitrogen). Immunofluorescent images were recorded with an IX71 inverted microscope (Olympus), and the signal intensities were quantified using Image Gauge software, version 4.22 (Fujifilm) and expressed in arbitrary units.

For immunoblotting of axonal proteins, the sciatic nerve segments 1 mm both proximal and distal to the ligated site were removed without paraformaldehyde fixation, and frozen in with powdered CO_2 in acetone. Protein extraction and Western blotting were performed as described above.

In situ *hybridization*. Formalin-fixed, paraffin-embedded 6-μm-thick sections of the spinal cord were deparaffinized, treated with proteinase K, and processed for *in situ* hybridization using an ISHR kit (Nippon Gene, Tokyo, Japan) according to the manufacturer's instructions. Dynactin 1 cDNA was obtained from spinal cords of wild-type mice. The primers, 5′-AGATGGTGGAGATGCTGACC-3′ and 5′-GAGCCTTGGTCTCAGCAAAC-3′, were phosphorylated with T4polynucleotide kinase (Stratagene Cloning Systems, La Jolla, CA). The cDNA was inserted into the pSPT 19 vector (Roche). Dioxigenin-labeled cRNA antisense and sense probes, 380 bp long, were generated from this plasmid using T7 and SP6 polymerase (Roche), respectively. Spinal cord sections were hybridized for 16 h at 42°C washed in formamide–4× SSC (50:50 v/v) at the same temperature, treated with RNase A at 37°C, and washed again in 0.1× SSC at 42°C. The signals were detected immunologically with alkaline phosphatase-conjugated anti-dioxigenin antibody and incubated with NBT/BCIP (Roche) for 16 h at 42°C. Slices were counterstained with methyl green. To quantify the intensity of the signals in the cell bodies of spinal motor neurons, three nonconsecutive sections from a wild-type littermate and those of a transgenic mouse from lines 7–8 or 4–6 were analyzed using the NIH Image program (version 1.62). Sections adjacent to those used for *in situ* hybridization were processed for immunohistochemistry using anti-polyglutamine antibody as described above.

Quantitative real-time PCR. Dynactin 1 mRNA levels were determined by real-time PCR as described before (Ishigaki et al., 2002; Ando et al., 2003). Briefly, total RNA (5 μg each) from AR-97Q and wild-type spinal cord were reverse transcribed into first-strand cDNA using SuperScript II reverse transcriptase (Invitrogen). Real-time PCR was performed in a total volume of 50 μl, containing 25 μl of 2× QuantiTect SYBR Green PCR Master Mix and 0.4 μM of each primer (Qiagen, Valencia, CA), and the product was detected by the iCycler system (Bio-Rad Laboratories, Hercules, CA). The reaction conditions were 95°C for 15 min and then 45 cycles of 15 s at 95°C followed by 60 s at 55°C. For an internal standard control, the expression level of glyceraldehyde-3-phosphate dehydrogenase (GAPDH) was simultaneously quantified. The following primers used were 5′-CTCAGAGGAGCCCAGATGA-3′ and 5′-GCTGGTCTTGCGGTACAGT-3′ for dynactin 1, 5′-GAGAGCATGGAGCTGGTGTA-3′ and 5′-CCAACCACGAAGTTGTTGAC-3′ for dynein intermediate chain, 5′-TACCAGGTGGGAGTGCATTA-3′ and 5′-CAGTCACTATGCCCATGACC-3′ for dynein heavy chain, 5′-ACAAGCGTGGAACACATCAT-3′ and 5′-TCTTTCCAATGCGATCTGAG-3′ for dynamitin, and 5′-CCTGGAGAAACCTGCCAAGTAT-3′ and 5′-TGAAGTCGCAGGAGACAACCT-3′ for GAPDH. The threshold cycle of each gene was determined as the number of PCR cycles at which the increase in reporter fluorescence was 10 times the baseline signal. The weight of the gene contained in each sample was equal to the log of the starting quantity and the standardized expression level in each mouse was equal to the weight ratio of each gene to that of GAPDH.

For the real-time PCR with mRNA extracted from SH-SY5Y cells, the following primers were used: 5′-CTTGGAAGCGATGAATGAGA-3′ and 5′-TAGTCTGCAACGTCTCCTG-3′ for dynactin 1, and 5′-AGCCTCAAGATCATCAGCAAT-3′ and 5′-GGACTGTGGTCATGAGTCCTT-3′ for GAPDH.

Plasmid vectors and cell culture. Human AR cDNAs containing 24 or 97 CAG repeats were subcloned into pcDNA3.1 (Invitrogen) as described previously (Kobayashi et al., 2000). Human dynactin 1 cDNA was also subcloned into pcDNA3.1 (Invitrogen). The human neuroblastoma cells (SH-SY5Y, #CRL-2266; American Type Culture Collection, Manassas, VA) were plated in 6-well dishes in 2 ml of DMEM/F12 containing 10% fetal bovine serum with penicillin and streptomycin, and each dish was transfected with 2 μg of the vector containing AR24, AR97, or mock and with 2 μg of the vector containing dynactin 1 or mock using Opti-MEM (Invitrogen) and Lipofectamine 2000 (Invitrogen) and then differentiated in differentiation medium (DMEM/F12 supplemented with 5% fetal calf serum and 10 μM retinoic acid) for 2 d. Two days after transfection, cells were stained with propidium iodide (Invitrogen, Eugene, OR) and mounted in Gelvatol. Quantitative analyses were made from triplicate determinations. Duplicate slides were graded blindly in two independent trials as described previously (Katsuno et al., 2005).

Statistical analyses. We analyzed data using the Kaplan-Meier and log-rank test for survival rate, ANOVA with *post hoc* test (Dunnett) for multiple comparisons, and an unpaired *t test* from Statview software version 5 (Hulinks, Tokyo, Japan).

Results

Accumulation of axonal proteins in distal motor axons of SBMA mouse

To clarify the molecular basis of neuronal dysfunction in SBMA, we analyzed histopathological alterations in the spinal cords of transgenic mice carrying full-length human *AR* with 97 CAGs (AR-97Q mice) (Katsuno et al., 2002, 2003). We first focused on the expression and phosphorylation level of NF-H because affected mice demonstrate axonal atrophy in the ventral nerve root (Katsuno et al., 2002). Although it has been widely accepted that NF-H phosphorylation is a crucial factor determining axon caliber, neither the amounts nor the phosphorylation levels of NF-H in spinal cord or ventral root were decreased in male AR-97Q mice compared with wild-type littermates (supplemental Fig. 1*A–C*, available at www.jneurosci.org as supplemental material). The distribution of NF-H in the anterior horn of AR-97Q mice was also indistinguishable from that of wild-type or AR-24Q mice bearing human AR with a normal polyglutamine length (Fig. 1*A*). However, AR-97Q mice demonstrated a striking accumulation of both phosphorylated and nonphosphorylated NF-H in skeletal muscle, a phenomenon not observed in AR-24Q or wild-types (Fig. 1*A*). Although motor neurons originating in the anterior horn are always affected in SBMA, because the primary motor neurons projecting their axons to the anterior horn are not affected, no accumulation is seen in this region. The damage to motor neurons originating within the anterior horn results in accumulation of NFs in the skeletal muscle, instead of the spinal cord. A similar accumulation of the middle molecular weight NF was also observed (data not shown). To clarify whether this phenomenon is specific to neurofilaments, we performed immunohistochemistry on both spinal cord and muscle with an antibody against synaptophysin, a transmembrane glycoprotein of synaptic vesicles that is also retrogradely transported in axons (Li et al., 1995). In AR-97Q mice, synaptophysin accumulated among the muscle fibers in a pattern similar to that of NF-H, whereas no such accumulation was observed in unaffected mice (Fig. 1*B*).

We then investigated the time course of abnormally accumulated NF in skeletal muscle. Because the onset of motor dysfunction occurs at 9–10 weeks in AR-97Q mice, NF pathology before and after the onset was examined. Anti-NF immunostaining demonstrated that intramuscular NF accumulation was detectable as early as 7 weeks before the onset of muscle weakness in this

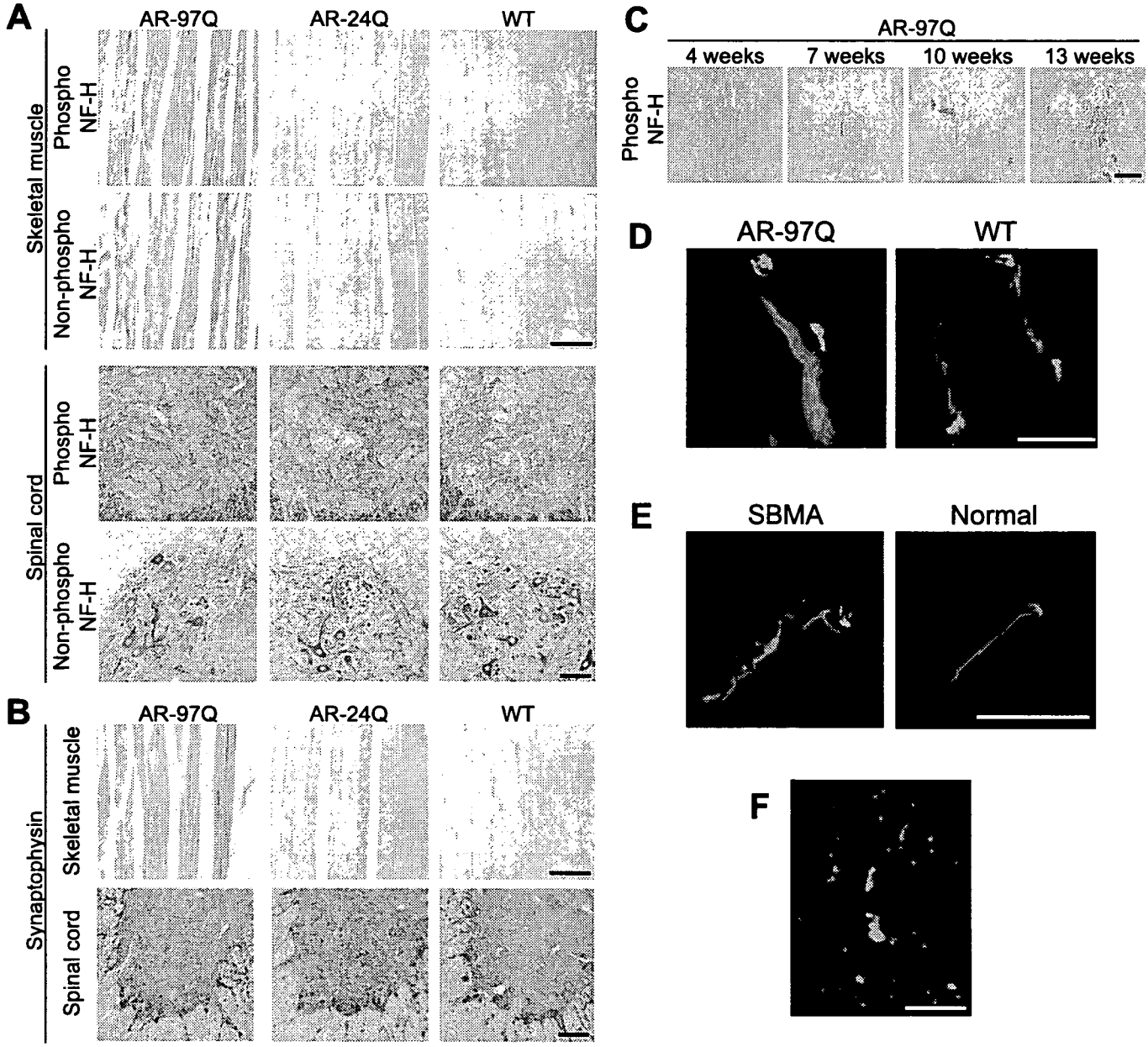

Figure 1. Accumulation of neurofilament and synaptophysin in the distal end of motor axons. ***A***, Immunohistochemistry of skeletal muscle and spinal cord from AR-97Q (4–6), AR-24Q, and wild-type mice (12 weeks) using an antibody for phosphorylated or nonphosphorylated NF-H. ***B***, Immunohistochemistry for synaptophysin shows findings parallel to those of neurofilament. ***C***, Age-dependent change in antiphosphorylated NF-H immunohistochemistry in skeletal muscle of SBMA mice. ***D***, Immunofluorescence of mouse skeletal muscle using α-bungarotoxin (green) in combination with antiphospho-NF-H antibody (red). Phosphorylated NF-H accumulates in the distal end of motor axons in AR-97 mice (7–8, 12 weeks). ***E***, Antiphospho-NF-H immunofluorescence with α-bungarotoxin staining in skeletal muscle from a human SBMA patient showing similar neurofilament accumulation. ***F***, Double-labeling of skeletal muscle from an AR-97Q mouse (4–6, 12 weeks) using antiphospho-NF-H antibody (green) and anti-AR (red) shows that accumulated NF-H does not colocalize with AR. Scale bars, 100 μm.

mouse model, and aggravated thereafter (Fig. 1*C*). These observations suggest that intramuscular accumulation of NF plays a role in the motor neuron dysfunction in this mouse model of SBMA.

To confirm the distribution of NF-H and synaptophysin in skeletal muscle, we examined the localization of these proteins in relation to the neuromuscular junction. Immunohistochemistry using α-bungarotoxin to mark the junctions, and fluorescent-labeled antibodies showed that both NF-H and synaptophysin accumulated in the most distal motor axon adjacent to neuromuscular junctions (Fig. 1*D*). A similar intramuscular accumulation of neurofilament was detected in the skeletal muscle of SBMA patients (Fig. 1*E*). Although pathogenic AR accumulated in the nuclei of skeletal muscle in the AR-97Q mice, the accumulation of NF-H did not colocalize with AR (Fig. 1*F*). Moreover, immunoprecipitation demonstrated no interaction between AR and NF-H (data not shown). These findings exclude the possibility that pathogenic AR directly interrupts the axonal trafficking.

Retrograde axonal transport is disrupted in SBMA mouse

To elucidate the molecular basis of the abnormal distribution of NF and synaptophysin, we studied axonal transport in this mouse model of SBMA. Axonal components undergo anterograde and/or retrograde axonal transport. Proteins including NF and synaptophysin are bidirectionally transported, whereas some

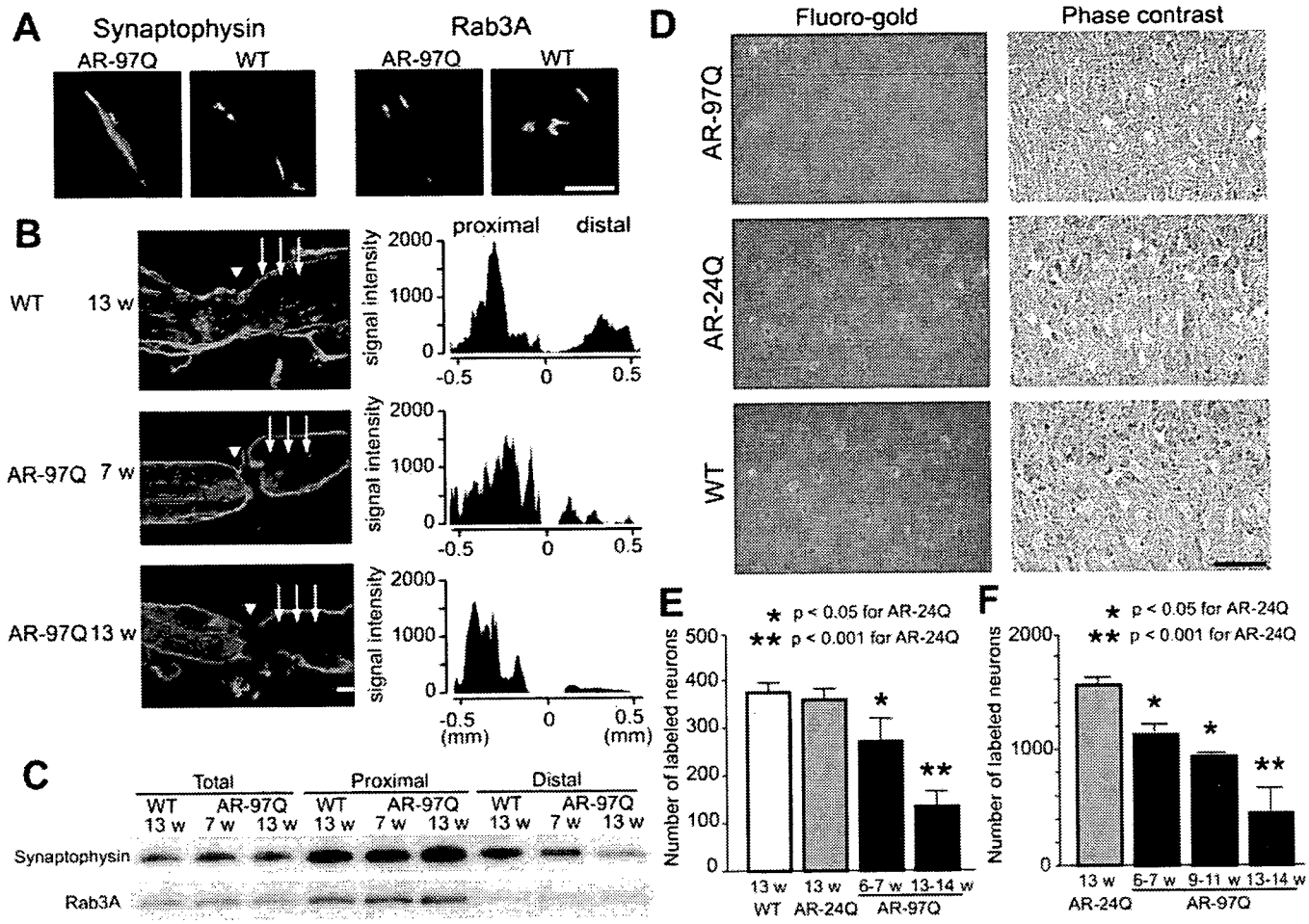

Figure 2. Perturbation of retrograde axonal transport in SBMA mice. ***A***, Immunofluorescence of mouse skeletal muscle using α-bungarotoxin (green) labeling the endplate together with anti-synaptophysin antibody (red) or anti-Rab3A antibody (red). Accumulation of Rab3A is not detected in wild-type or AR-97Q mice (7–8, 12 weeks). ***B***, Immunohistochemistry for synaptophysin in the sciatic nerve 8 h after ligation and representative quantification of immunoreactivity. Accumulation of synaptophysin immunoreactivity is decreased on the distal side (arrows) of the ligation site (arrowhead) in preonset (7 weeks) and advanced stage (13 weeks) AR-97Q mice. ***C***, Immunoblots of the sciatic nerve segments on both proximal and distal sides of the ligation. The total amount of proteins extracted from the contralateral nonligated sciatic nerve was analyzed as a control. ***D***, ***E***, Retrograde labeling of lumbar motor neurons of AR-97Q (7–8), AR-24Q, or wild-type mice (12 weeks) by Fluoro-gold injection into the gastrocnemius muscle (***D***) and the number of labeled neurons (***E***) ($n = 5$ for each group). ***F***, The number of motor neurons labeled by Fluoro-gold using the sciatic nerve stump method ($n = 5$ for each group). Scale bars: ***A***, ***B***, ***D***, 100 μm. Error bars indicate SD.

components such as Rab3A, a small GTP binding protein, are transported only anterogradely (Li et al., 1995; Roy et al., 2000). The distribution of Rab3A in skeletal muscle of SBMA mice was equivalent to that of wild-type mice, whereas synaptophysin and neurofilaments accumulated in the most distal motor axons of the SBMA mice only (Figs. 1*D*, 2*A*).

To further examine the nature of the axonal transport anomaly in SBMA mice, the sciatic nerve was ligated at mid-thigh level. Because the transport rate of NF is slower than other axonal components, we analyzed the transport of synaptophysin and Rab3A in this ligation study (Fig. 2*B*,*C*). In wild-type mice, synaptophysin accumulated predominantly on the proximal side of the ligation, but also on the distal side. Although synaptophysin and Rab3A accumulations proximal to the site of ligation were notable in both preonset and advanced stages of AR-97Q mice, their accumulation on the distal side was decreased before the onset of symptoms and was progressively inhibited. These findings suggest that disrupted retrograde axonal transport gives rise to the accumulation of axonal proteins in the distal motor axon terminals of SBMA mice before the onset of motor impairment.

To confirm this hypothesis, we analyzed retrograde neuronal labeling with the fluorescent tracer Fluoro-gold after its injection into the mouse calf muscle. The number of Fluoro-gold-labeled spinal motor neurons was significantly less in affected AR-97Q mice compared with AR-24Q or wild-type mice (Fig. 2*D*,*E*). To exclude the possibility that synaptic pathology contributed to diminished uptake of the tracer, we also examined Fluoro-gold labeling using direct application of the tracer into the sciatic nerve stump (Sagot et al., 1998). Again, AR-97Q mice showed fewer motor neurons labeled by Fluoro-gold applied directly to the proximal stump of the sciatic nerve than did the AR-24Q mice (Fig. 2*F*), suggesting that neither synaptic retraction nor disconnection is the basis for disruption of axonal transport. Furthermore, it should be noted that the decrease in the number of labeled neurons preceded the onset of motor symptoms in both of these experiments. These observations suggest that the disruption of retrograde transport plays an early role in the pathogenesis of motor neuron degeneration in SBMA.

Transcriptional dysregulation of dynactin 1 in SBMA

Retrograde axonal transport is microtubule-dependent and is regulated by the axon motor protein dynein and its associated protein complex, dynactin. To elucidate the molecular

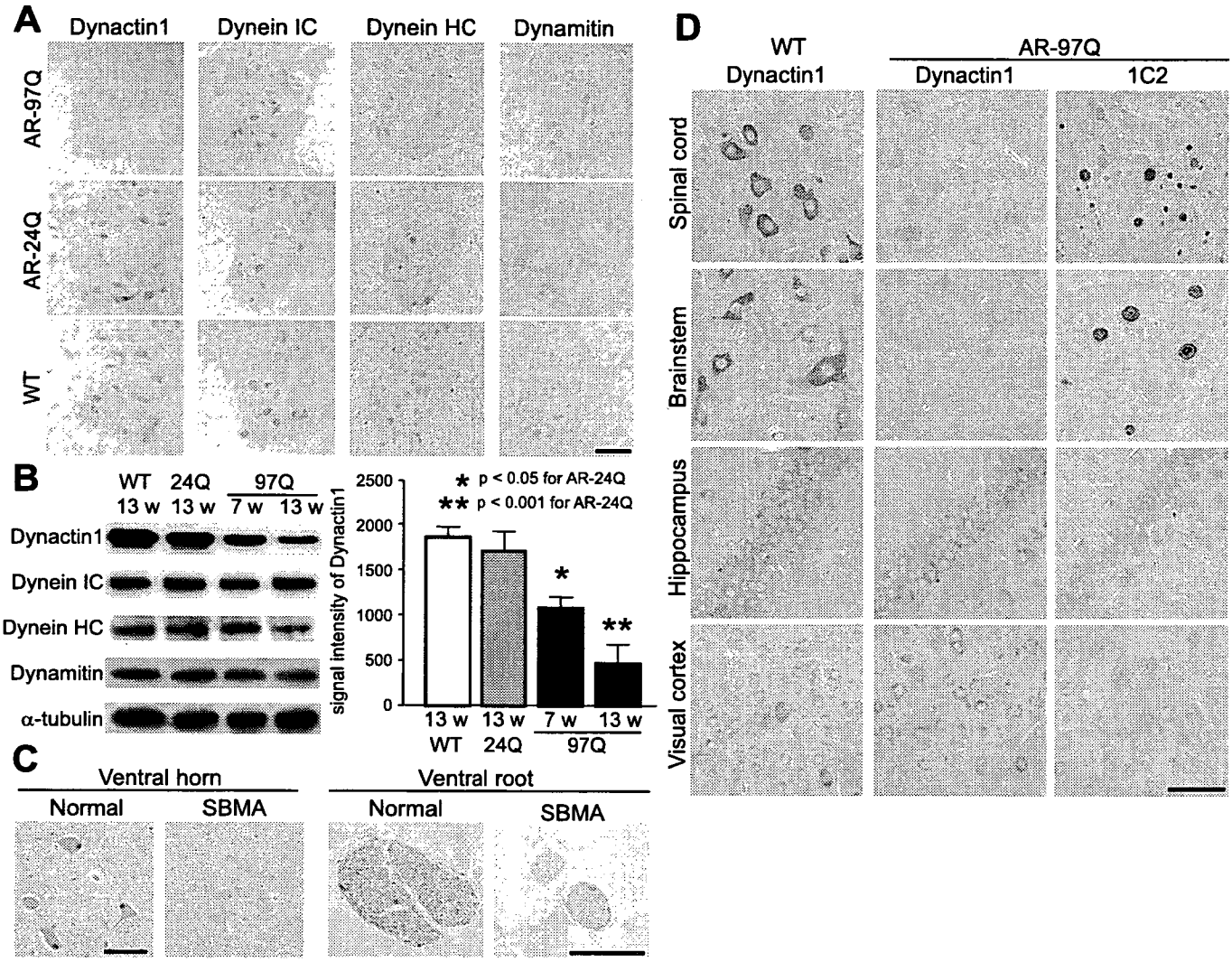

Figure 3. Decreased levels of dynactin 1 in SBMA. ***A***, Immunohistochemistry for motor proteins regulating retrograde axonal transport, dynactin 1, dynein intermediate chain (IC), dynein heavy chain (HC), and dynamitin in the spinal cord from AR-97Q (4–6), AR-24Q, and wild-type mice (12 weeks). Dynactin 1 is markedly diminished in the motor neurons of AR-97Q mice. ***B***, Western blot analysis for motor proteins in the ventral spinal root from presymptomatic or advanced AR-97Q mice (4–6) compared with those from AR-24Q and wild-type mice. ***C***, Dynactin 1 immunohistochemistry in the anterior horn and the ventral root of an SBMA patient and a normal subject. ***D***, Anti-dynactin 1 immunohistochemistry in various affected (spinal cord and brainstem) and nonaffected (hippocampus and visual cortex) tissues from wild-type and AR-97Q mice. Data from AR-97Q mice are compared with immunohistochemistry using the anti-polyglutamine antibody, 1C2. Scale bars: ***A***, 100 μm; ***C***, ***D***, 50 mm. Error bars indicate SD.

mechanism compromising retrograde axonal transport in SBMA mice, we examined the levels of various dynein and dynactin protein subunits. Immunohistochemistry of spinal cord sections demonstrated that the spinal motor neurons from AR-97Q mice had lower levels of dynactin 1, the largest subunit of dynactin, than did those from either wild-type or AR-24Q mice (Fig. 3*A*). In the ventral root, significantly decreased levels of dynactin 1 were apparent before the onset of motor symptoms (Fig. 3*B*). Although the level of dynein heavy chain was diminished in the advanced disease stage in SBMA mice, this phenomenon was not observed before the onset of symptoms (Fig. 3*B*). No alterations were observed in the levels of dynein intermediate chain or dynamitin, the p50 subunit of dynactin, throughout the disease course (Fig. 3*A*,*B*). To confirm the role of dynactin 1 in the pathogenesis of human SBMA, we also examined the protein level in autopsy specimens. As observed in the mouse model, the protein level of dynactin 1 was decreased in the anterior horn cells and in the ventral roots of SBMA patients (Fig. 3*C*).

To examine the cell specificity of reduced dynactin 1 levels we compared anti-dynactin 1 immunohistochemistry with that of anti-polyglutamine using the 1C2 antibody in various tissues from wild-type and AR-97Q mice (Fig, 3*D*). The immunoreactivity of dynactin 1 was markedly diminished in 1C2-positive tissues, but not in those lacking nuclear polyglutamine staining. This observation suggests that the reduction in dynactin 1 is relevant to the polyglutamine-mediated neuropathology. In addition, to investigate whether reduced levels of dynactin 1 were correlated with defective retrograde axonal transport, we analyzed anti-dynactin 1 immunohistochemistry in spinal cord sections labeled by Fluoro-gold (supplemental Fig. 2, available at www.jneurosci.org as supplemental material). The levels of dynactin 1 were decreased in the spinal motor neurons of AR-97Q mice concomitantly with decreased intensities of Fluoro-gold labeling. Together, these data strongly suggest that depletion of dynactin 1 is responsible for the disruption of retrograde axonal transport in SBMA.

To clarify the pathological mechanism responsible for reduc-

ing the levels of dynactin 1 protein in SBMA, mRNA levels were determined by *in situ* hybridization in AR-97Q and wild-type mice. Although dynactin 1 mRNA was expressed in virtually all motor neurons in the anterior horn, the expression was markedly repressed in AR-97Q mice (Fig. 4*A*). Moreover, the levels of dynactin 1 mRNA were significantly lower in those motor neurons demonstrating nuclear accumulation of pathogenic AR compared with those without 1C2 nuclear staining (Fig. 4*B*). Real-time quantitative PCR also demonstrated a significant decrease in dynactin 1 mRNA levels in the spinal cords of AR-97Q mice at all disease stages compared with those of wild-types (Fig. 4*C*). The level of dynein heavy chain mRNA was decreased in the advanced stage, but not in the preonset period. The levels of dynein intermediate chain mRNA and dynamitin mRNA were not altered either before or after the onset of motor symptoms.

To investigate the role that diminished levels of dynactin 1 play in neurodegeneration in SBMA, we tested whether overexpression of this protein suppressed the cellular toxicity usually observed in the presence of expanded polyglutamine. In SH-SY5Y cells bearing truncated AR containing an expanded polyglutamine, the level of dynactin 1 was decreased both in mRNA and in protein (Fig. 4*D*,*E*). In this cellular model of SBMA, overexpression of dynactin 1 alleviated cell death exerted by pathogenic AR (Fig. 4*E*).

In SBMA mice, the level of dynactin 1 protein in spinal motor neurons was restored by oral administration of sodium butyrate, an HDAC inhibitor that increases the level of histone acetylation leading to promotion of gene transcription (supplemental Fig. 3, available at www.jneurosci.org as supplemental material) (Minamiyama et al., 2004). Sodium butyrate-mediated upregulation of dynactin 1 also eventually alleviated the neurofilament accumulation in skeletal muscle (supplemental Fig. 3, available at www.jneurosci.org as supplemental material), although this treatment had no influence on the subcellular distribution of pathogenic AR protein (Minamiyama et al., 2004). These observations indicate that nuclear accumulation of aberrant AR in the nuclei of motor neurons leads to a decrease at the transcription level of dynactin 1, resulting in perturbation of retrograde axonal transport and subsequent motor neuron dysfunction.

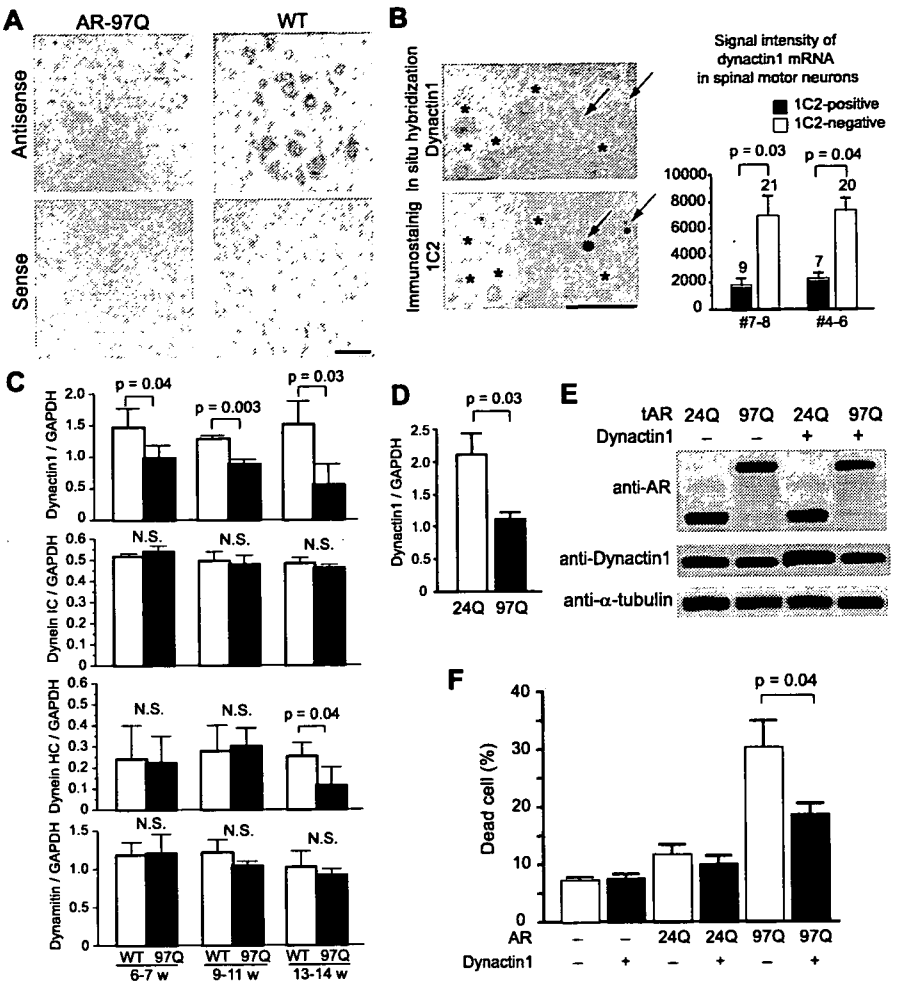

Figure 4. Transcriptional dysregulation of dynactin 1 in spinal motor neurons of SBMA mouse and effects of dynactin 1 overexpression. ***A***, *In situ* hybridization of dynactin 1 mRNA in the anterior horn of wild-type and AR-97 (4–6, 9 weeks) transgenic mice. Note the marked decrease in dynactin 1 mRNA levels in the spinal motor neurons of AR-97Q compared with those in wild-type mice. ***B***, *In situ* hybridization of dynactin 1 in the anterior horn. The adjacent sections were processed for anti-polyglutamine using the 1C2 antibody and the signals were quantified in representative AR-97Q mice (7–8, 9 weeks; 4–6, 10 weeks). Dynactin 1 mRNA expression is markedly decreased in the motor neurons demonstrating nuclear accumulation of pathogenic AR (arrows), but not in those lacking clear nuclear staining with anti-polyglutamine antibody (asterisks). The number above each bar indicates cell count. ***C***, The mRNA levels of dynactin 1 and other motor proteins in the spinal cords of wild-type and AR-97Q mice (7–8, 13 weeks) ($n = 4$ for each group) demonstrated by real-time, RT-PCR. Data shown are ratios of the various mRNA levels to GAPDH mRNA levels. ***D***, The mRNA levels of dynactin 1 in SH-SY5Y cells expressing either AR-24Q or AR-97Q ($n = 4$). ***E***, Immunoblots of SH-SY5Y cells expressing either AR-24Q or AR-97Q with or without overexpression of exogenous dynactin 1. ***F***, Frequency of cell death detected by propidium iodide staining. Dynactin 1 overexpression significantly reduced cell death in the cells bearing AR with elongated polyglutamine. Scale bars: ***A***, ***B***, 100 μm. Error bars indicate SD ($n = 6$ for each group). IC, Intermediate chain; HC, heavy chain.

Castration reverses symptoms and pathology of SBMA mouse

To examine the reversibility of the phenotypes resulting from polyglutamine-induced neuronal dysfunction, we investigated the effect of castration on early symptomatic SBMA mice. Male AR-97Q mice (7–8 and 4–6) demonstrate a rapid aggravation of neuromuscular phenotypes and usually succumb 3–4 weeks after the onset of motor impairment. The motor-impaired phenotype of the SBMA mouse is dependent on circulating testosterone levels, and we reported previously that castration during the presymptomatic period (4 weeks), to eliminate testosterone, drastically prevents the development of neurological symptoms such as weakness, amyotrophy, and shortened life span (Katsuno et al., 2002). In the present study, we castrated male AR-97Q mice within 1 week after the onset of rotarod task impairment. Castration reversed motor dysfunction in AR-97Q mice, even though it was performed after the onset of symptoms (Fig. 5*A*). Most mice showed a reduction in daily activity and body weight loss at the onset of rotarod task defect; these symptoms were also reversed by castration. In accordance with these observations,

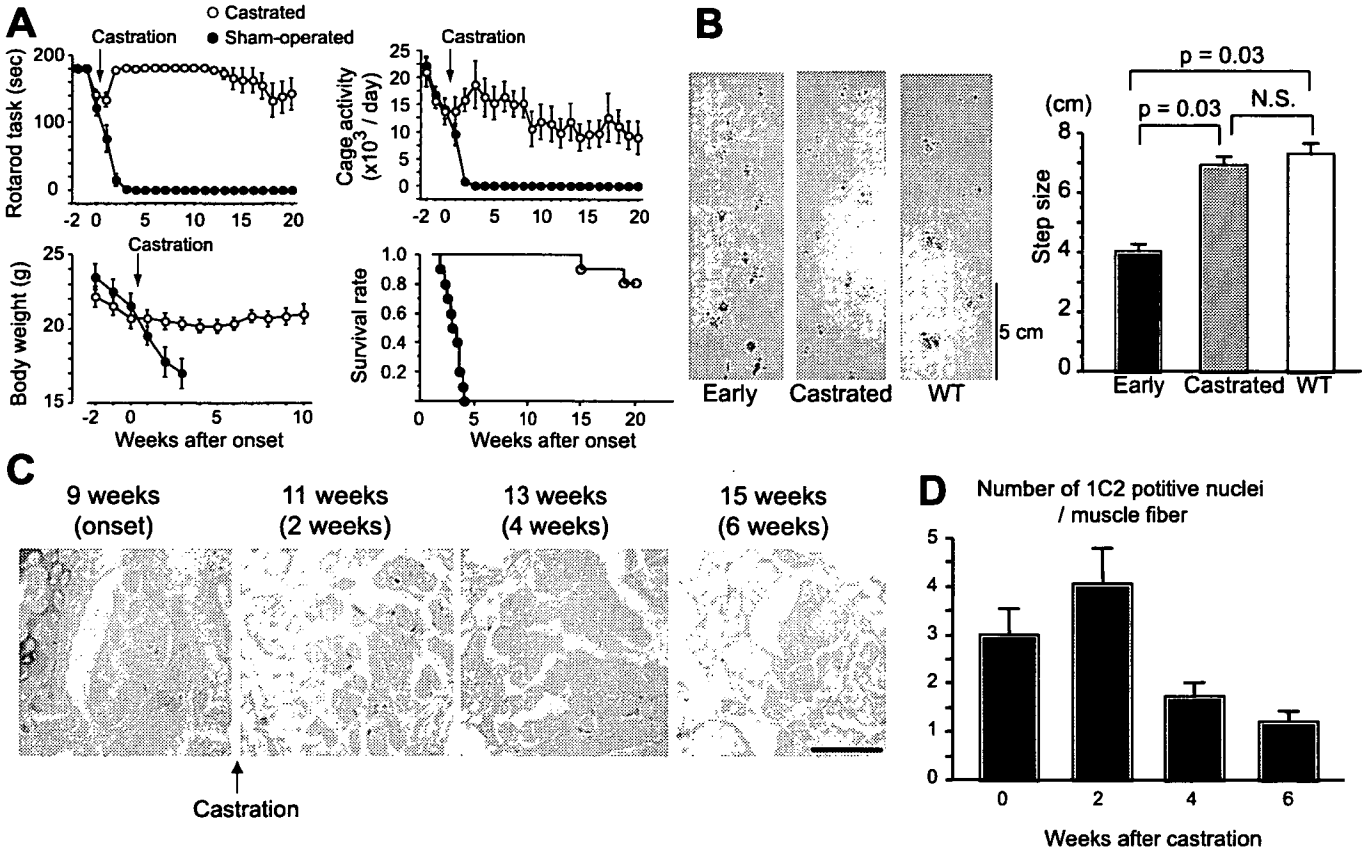

Figure 5. Symptomatic and histopathological reversibility of the SBMA phenotype in AR-97Q mice. ***A***, Castration of early symptomatic AR-97Q mice within 1 week after symptomatic manifestation resulted in significant improvement of the symptomatic phenotypes: rotarod task (7–8), cage activity (4–6), body weight (4–6), and survival rate (4–6). There are significant differences in all parameters between the sham-operated ($n = 10$) and castrated ($n = 10$) male AR-97Q mice ($p < 0.0001$, $p < 0.0001$, $p = 0.0001$, and $p = 0.0006$, respectively). ***B***, Representative footprints of an individual AR-97Q mouse (2–6) at the early onset of motor symptoms and after he had been castrated within 1 week after the onset of rotarod impairment, compared with those of a wild-type mouse. Quantification of the gait stride data ($n = 4$). ***C***, Nuclear accumulation of pathogenic AR with expanded polyglutamine in the tail muscle of one individual male AR-97Q mouse (4–6). ***D***, Castration after motor impairment onset significantly reduced the number of nuclei stained by an anti-polyglutamine antibody, 1C2 ($n = 4$). Scale bar: ***C***, 100 μm. Error bars indicate SD.

postonset castration significantly prolonged the life span of the male AR-97Q mice. We confirmed the reversal of motor symptoms by analyzing gait strides in a series of mouse footsteps (Fig. 5*B*).

To confirm the rescue effects of castration on histopathology, we investigated the nuclear accumulation of pathogenic AR in the skeletal muscle of tail sections sampled over time from the same mouse. Although the number of nuclei positively stained with 1C2 continued to increase for 2 weeks after the castration, at 4 weeks there was a significant decrease in expanded polyglutamine AR-positive nuclei (Fig. 5*C*,*D*). This time course corresponds approximately to the that of the symptomatic improvements, suggesting that nuclear accumulation of pathologic AR contributes to neuronal dysfunction and consequent symptomatic manifestation in SBMA mice.

Castration reverses dynactin 1 expression and restores retrograde axonal transport

It is important to determine whether disrupted retrograde axonal transport resulting from transcriptional dysregulation of dynactin 1, contributes to the reversible motor neuronal dysfunction in the early disease stage of SBMA mice. We therefore investigated axonal transport and the level of dynactin 1 expression in transgenic mice within 1 week after the onset of rotarod task impairment. In this early stage of the disease, the mice already demonstrated a reduction in the number of spinal motor neurons labeled by Fluoro-gold (Fig. 6*A*). Castration of symptomatic AR-97Q mice restored Fluoro-gold staining in the spinal motor neurons to a similar level as seen in wild-types (compare Figs. 2*D*, 6*A*). Castration after the onset of muscle weakness reduced the intramuscular accumulation of neurofilaments and synaptophysin in AR-97Q mice (Fig. 6*B*,*C*). Immunohistochemistry of spinal cord showed that postsymptomatic castration also eliminated nuclear accumulation of pathogenic AR as detected by the 1C2 antibody, and restored anti-dynactin 1 immunoreactivity in motor neurons (Fig. 6*D*). Immunoblotting demonstrated that the level of dynactin 1 protein, but not that of dynein heavy chain, was decreased in the ventral root of AR-97Q mice in the early symptomatic stage (Fig. 6*E*). Castration after the onset of motor impairment restored dynactin 1 to its normal levels in the ventral root, whereas it had no effect on dynactin 1 expression in wild-type mice (Fig. 6*E*). These observations indicate that the castration-mediated restoration of dynactin 1 expression improves retrograde axonal transport and contributes to the reversal of neuromuscular phenotypes in SBMA mice at an early stage of the disease process.

Discussion

Reversibility of neuronal dysfunction in SBMA

The fundamental pathological feature of polyglutamine diseases is the loss of neurons in selected regions of the CNS. Neuronal cell death, however, is often undetectable in mildly affected HD pa-

tients despite the presence of definite clinical features (Vonsattel et al., 1985). The early HD symptoms may thus result from functional alterations within neurons rather than cell death (Walker et al., 1984). In mouse models of polyglutamine diseases, it has been postulated that neuronal dysfunction, without cell loss, is sufficient to cause neurological symptoms (Mangiarini et al., 1996; Clark et al., 1997). These observations indicate that the pathogenesis of polyglutamine diseases is potentially reversible at an early stage. This hypothesis is supported by the observation that arrest of gene expression after the onset of symptoms reverses behavioral and neuropathological abnormalities in conditional mouse models of polyglutamine diseases (Yamamoto et al., 2000; Zu et al., 2004). The present study supports this hypothesis in that castration after the onset of motor deficit reverses behavioral and histopathological abnormalities by preventing nuclear accumulation of the pathogenic AR protein. These findings imply that cellular protective responses successfully abrogate the toxicity of polyglutamine-containing pathogenic protein, unless it perpetually accumulates in the nucleus.

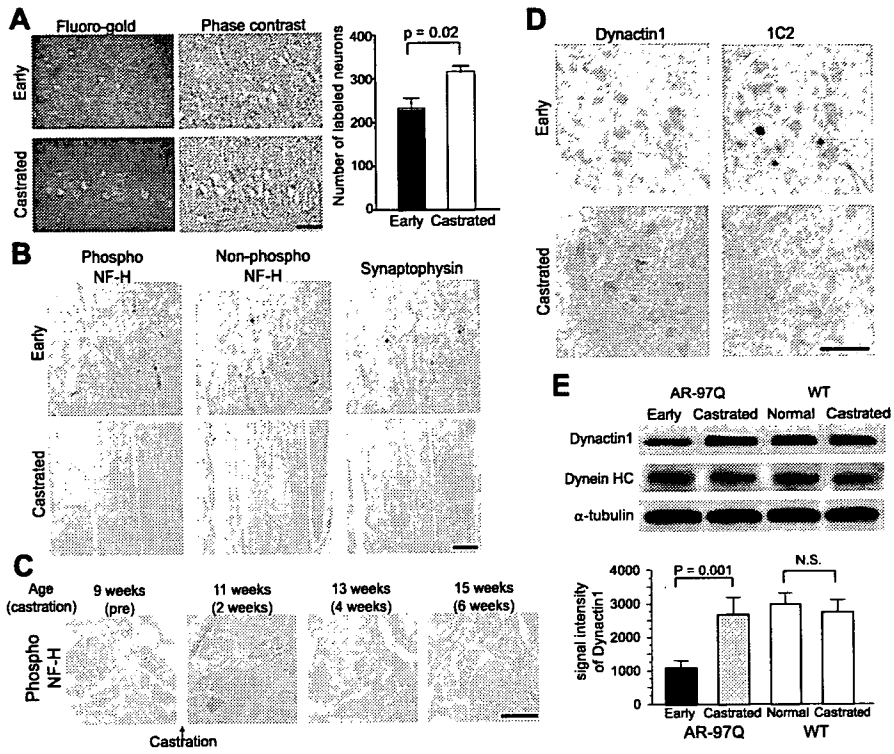

Figure 6. Hormonal intervention restores expression level of dynactin 1 and improves axonal transport. ***A***, Fluoro-gold labeling of spinal cord from early symptomatic (7–8; 9–11 weeks) and castrated (7–8; 13–16 weeks) male AR-97Q mice ($n = 5$ for each group). ***B***, Immunohistochemistry of skeletal muscle for NF-H and synaptophysin. ***C***, Immunohistochemistry for phosphorylated NF-H in the tail muscle of an individual male AR-97Q mouse (4–6). Castration after onset of symptoms depletes NF-H accumulation in the skeletal muscle. ***D***, Immunohistochemistry of the spinal cords of early symptomatic (4–6; 11 weeks) and castrated (4–6; 15 weeks) male AR-97Q mice using anti-dynactin 1 and 1C2. Castration eliminated nuclear accumulation of expanded polyglutamine AR. ***E***, Immunoblots of ventral roots from early symptomatic (4–6; 11 weeks) and castrated (4–6; 15 weeks) AR-97Q mice together with that from wild-type littermates (15 weeks) using antibodies against dynactin 1, dynein heavy chain (HC), and α-tubulin. Scale bars: ***A–D***, 100 μm. Error bars indicate SD ($n = 3$ for each group).

Protein quality control systems, including molecular chaperones, the ubiquitin-proteasome system, and autophagy have been shown to reduce polyglutamine toxicity in various animal models of polyglutamine diseases (Adachi et al., 2003; Ravikumar et al., 2004; Katsuno et al., 2005; Waza et al., 2005). It is thus logical that inhibition of AR translocation into the nucleus restores the protein degradation machinery, such as ubiquitin-proteasome system, leading to the reduction in the amount of aggregates as well as the improvement of neuronal dysfunction in the SBMA mice (Waza et al., 2005).

Defective retrograde axonal transport in SBMA

The SBMA mice we examined demonstrated impairment of retrograde axonal transport, resulting in the accumulation of neurofilaments and synaptophysin in the distal motor axon. Many proteins required for neuronal survival are synthesized within neuronal perikarya and are transported along the axon toward the synaptic terminals (Shea, 2000). A bidirectional delivery system consisting of anterograde and retrograde transport enables the recycling of cytoskeletons and synaptic vesicle-associated proteins. A histopathological hallmark of amyotrophic lateral sclerosis (ALS) is the accumulation of neurofilaments in cell bodies and proximal axons of affected motor neurons, presumably caused by compromised anterograde axonal transport; nevertheless, this finding has not been observed in SBMA (Sobue et al., 1990; Julien 2001). Transgenic SBMA mice demonstrate marked neurofilament storage in the distal motor axons, but not in the proximal axons or cell bodies. Neurofilament accumulation at motor endplates has also been reported in a transgenic mouse model of spinal muscular atrophy, another lower motor neuron disease (Cifuentes-Diaz et al., 2002). Axonal transport of NF depends on the dynein/dynactin system, disruption of which results in accumulation of neurofilaments at the distal axon in both cultured cells and transgenic mice (LaMonte et al., 2002; He et al., 2005). When combined, these findings indicate that the accumulation of axonal components in distal motor axons appears to be a substantial pathology associated with degeneration of lower motor neurons.

In the present study, synaptophysin showed an accumulation pattern similar to that of neurofilaments, whereas the distribution of Rab3A, another synaptic vesicle-associated protein, was not altered in this mouse model. Crush injury experiments have shown that although both proteins are delivered from cell bodies into axons, of the two only synaptophysin undergoes retrograde transport (Li et al., 1995, 2000). In addition, Fluoro-gold labeling experiments clearly demonstrated the disruption of retrograde, but not anterograde axonal transport in the spinal motor neurons of SBMA mice before the onset of muscle weakness. Together, the pathogenesis of motor neuronal dysfunction in SBMA is likely to be based on the perturbation of retrograde axonal transport, and not on an excessive transport of total axonal proteins.

Axonal transport impairment has been implicated in the pathogenesis of HD and SBMA (Gunawardena et al., 2003; Szebenyi et al., 2003). Although axonal inclusion interferes with axonal transport in a cell model of SBMA (Piccioni et al., 2002), AR containing expanded polyglutamine may also inhibit anterograde and/or retrograde axonal transport without visible aggregate formation (Szebenyi et al., 2003; Morfini et al., 2006). Accu-

mulation of neurofilaments at nerve terminals has also been documented in a mouse model of HD (Ribchester et al., 2004). In our SBMA mice, pathogenic AR did not colocalize with accumulated neurofilament, nor did it form axonal inclusions. More intriguingly, sodium butyrate-mediated gene upregulation attenuated the accumulation of neurofilaments, but did not alter the intracellular distribution of AR. These observations suggest that the defective retrograde axonal transport in SBMA mice does not result from the direct interaction between aberrant AR and axonal components, but rather from a secondary mechanism resulting from expanded polyglutamine.

Dynactin in motor neuron disease

The present study indicates that a decrease in the level of dynactin 1, the p150 subunit of dynactin, in affected neurons is a fundamental early event in the pathogenesis of SBMA. Dynactin is a multiprotein complex regulating dynein, a microtubule-dependent molecular motor for retrograde axonal transport. A mutation in *DCTN1*, the gene encoding dynactin 1, has been identified in a family with an autosomal dominant form of lower motor neuron disease and in another with ALS (Puls et al., 2003; Münch et al., 2005). A gene expression analysis of sporadic ALS patients revealed a significant decrease in dynactin 1 mRNA (Jiang et al., 2005). Overexpression of dynamitin dissociates the dynactin complex, resulting in late-onset motor neuron degeneration in a transgenic mouse model of motor neuron disease (LaMonte et al., 2002). These observations specifically link an impaired dynactin function to the pathogenesis of motor neuron diseases.

The pathological alteration in individual polyglutamine diseases is limited to distinct subsets of neurons, suggesting that the causative protein context influences the distribution of lesions. Motor neurons are selectively affected in SBMA, although pathogenic ARs are expressed in a wide range of neuronal and non-neuronal tissues (Doyu et al., 1994). A decreased level of dynactin 1 may contribute to this pathological selectivity, because a mutation in the *DCTN1* gene causes a lower motor neuron disease resembling SBMA (Puls et al., 2003, 2005).

Link between altered transcription and neuronal dysfunction

Numerous studies have shown that nuclear accumulation of pathogenic polyglutamine-proteins is essential for neurodegeneration, although cytoplasmic events may also contribute to the pathogenesis (Gatchel and Zoghbi, 2005). Polyglutamine aggregation sequesters a variety of fundamental cellular factors including heat shock proteins and proteasomal components as well as transcriptional factors and coactivators. cAMP response element-binding protein-binding protein (CBP), a transcriptional coactivator, colocalizes with intranuclear inclusions in SBMA patients as well as in transgenic SBMA mice (McCampbell et al., 2000; Nucifora et al., 2001). In addition to its sequestration in inclusion bodies, the histone acetyltransferase activity of CBP is also inhibited by soluble polyglutamine-protein (Steffan et al., 2001). This theory suggests that HDAC inhibitors, which upregulate transcription through acetylation of nuclear histone, may open new avenues in the development of therapeutics. In a fly model of HD, the HDAC inhibitors, sodium butyrate and suberoylanilide hydroxamic acid, increased histone acetylation, leading to the mitigation of neurodegeneration (Steffan et al., 2001). These compounds also improve motor dysfunction in mouse models of HD and SBMA (Hockly et al., 2003; Minamiyama et al., 2004).

In the present study, a reduction in the level of dynactin 1 protein is ascribed to polyglutamine-mediated transcriptional dysregulation, because the mRNA level of this protein is decreased in expanded polyglutamine AR-positive spinal motor neurons. It should be noted that this diminution was significant in the neurons demonstrating nuclear accumulation of pathogenic AR, implying that polyglutamine-induced transcriptional perturbation underlies this pathological process. This hypothesis is confirmed by the observation that administration of sodium butyrate, an HDAC inhibitor, restores dynactin 1 expression, resulting in elimination of neurofilament accumulation at distal motor axons. Although, because of the nonspecific nature of sodium butyrate, we cannot at this time rule out the possibility that expression of some other protein was also elevated, leading to the elimination of neurofilament accumulation.

Given that the expression of other axon motor proteins regulating retrograde axonal transport, such as dynein intermediate chain, dynein heavy chain and dynamitin are not altered before the onset of symptoms, the reduction in dynactin 1 appears to instigate the neurodegeneration in SBMA. In addition to our study, the selective perturbation of certain subsets of gene transcription has been demonstrated in other animal models of polyglutamine diseases (Sugars and Rubinsztein 2003; Sopher et al., 2004), although the precise mechanism has yet to be elucidated.

In summary, the present study demonstrates that the pathogenesis of SBMA is a reversible dysfunction of motor neurons that occurs in the early stages of the disease. Polyglutamine-induced transcriptional alteration of dynactin 1 appears to disrupt retrograde axonal transport, contributing to the early reversible neuronal dysfunction. These observations suggest that transcriptional alteration and subsequent involvement of retrograde axonal transport are substantial therapeutic targets for SBMA.

References

Adachi H, Katsuno M, Minamiyama M, Sang C, Pagoulatos G, Angelidis C, Kusakabe M, Yoshiki A, Kobayashi Y, Doyu M, Sobue G (2003) Heat shock protein 70 chaperone overexpression ameliorates phenotypes of the spinal and bulbar muscular atrophy transgenic mouse model by reducing nuclear-localized mutant androgen receptor protein. J Neurosci 23:2203–2211.

Adachi H, Katsuno M, Minamiyama M, Waza M, Sang C, Nakagomi Y, Kobayashi Y, Tanaka F, Doyu M, Inukai A, Yoshida M, Hashizume Y, Sobue G (2005) Widespread nuclear and cytoplasmic accumulation of mutant androgen receptor in SBMA patients. Brain 128:659–670.

Ando Y, Liang Y, Ishigaki S, Niwa J, Jiang Y, Kobayashi Y, Yamamoto M, Doyu M, Sobue G (2003) Caspase-1 and -3 mRNAs are differentially upregulated in motor neurons and glial cells in mutant SOD1 transgenic mouse spinal cord: a study using laser microdissection and real-time RT-PCR. Neurochem Res 28:839–846.

Banno H, Adachi H, Katsuno M, Suzuki K, Atsuta N, Watanabe H, Tanaka F, Doyu M, Sobue G (2006) Mutant androgen receptor accumulation in spinal and bulbar muscular atrophy scrotal skin: a pathogenic marker. Ann Neurol 59:520–526.

Cha JH (2000) Transcriptional dysregulation in Huntington's disease. Trends Neurosci 23:387–392.

Chevalier-Larsen ES, O'Brien CJ, Wang H, Jenkins SC, Holder L, Lieberman AP, Merry DE (2004) Castration restores function and neurofilament alterations of aged symptomatic males in a transgenic mouse model of spinal and bulbar muscular atrophy. J Neurosci 24:4778–4786.

Cifuentes-Diaz C, Nicole S, Velasco ME, Borra-Cebrian C, Panozzo C, Frugier T, Millet G, Roblot N, Joshi V, Melki J (2002) Neurofilament accumulation at the motor endplate and lack of axonal sprouting in a spinal muscular atrophy mouse model. Hum Mol Genet 11:1439–1447.

Clark HB, Burright EN, Yunis WS, Larson S, Wilcox C, Hartman B, Matilla A, Zoghbi HY, Orr HT (1997) Purkinje cell expression of a mutant allele of

SCA1 in transgenic mice leads to disparate effects on motor behaviors, followed by a progressive cerebellar dysfunction and histological alterations. J Neurosci 17:7385–7395.

Doyu M, Sobue G, Kimata K, Yamamoto K, Mitsuma T (1994) Androgen receptor mRNA with increased size of tandem CAG repeat is widely expressed in the neural and nonneural tissues of X-linked recessive bulbospinal neuronopathy. J Neurol Sci 127:43–47.

Gatchel JR, Zoghbi HY (2005) Diseases of unstable repeat expansion: mechanism and principles. Nat Rev Genet 6:743–755.

Gunawardena S, Her LS, Brusch RG, Laymon RA, Niesman IR, Gordesky-Gold B, Sintasath L, Bonini NM, Goldstein LS (2003) Disruption of axonal transport by loss of huntingtin or expression of pathogenic polyglutamine proteins in *Drosophila*. Neuron 40:25–40.

He Y, Francis F, Myers KA, Yu W, Black MM, Baas PW (2005) Role of cytoplasmic dynein in the axonal transport of microtubules and neurofilaments. J Cell Biol 168:697–703.

Hockly E, Richon VM, Woodman B, Smith DL, Zhou X, Rosa E, Sathasivam K, Ghazi-Noori S, Mahal A, Lowden PA, Steffan JS, Marsh JL, Thompson LM, Lewis CM, Marks PA, Bates GP (2003) Suberoylanilide hydroxamic acid, a histone deacetylase inhibitor, ameliorates motor deficits in a mouse model of Huntington's disease. Proc Natl Acad Sci USA 100:2041–2046.

Ishigaki S, Liang Y, Yamamoto M, Niwa J, Ando Y, Yoshihara T, Takeuchi H, Doyu M, Sobue G (2002) X-linked inhibitor of apoptosis protein is involved in mutant SOD1-mediated neuronal degeneration. J Neurochem 82:576–584.

Jiang YM, Yamamoto M, Kobayashi Y, Yoshihara T, Liang Y, Terao S, Takeuchi H, Ishigaki S, Katsuno M, Adachi H, Niwa J, Tanaka F, Doyu M, Yoshida M, Hashizume Y, Sobue G (2005) Gene expression profile of spinal motor neurons in sporadic amyotrophic lateral sclerosis. Ann Neurol 57:236–251.

Julien JP (2001) Amyotrophic lateral sclerosis: unfolding the toxicity of the misfolded. Cell 104:581–591.

Katsuno M, Adachi H, Kume A, Li M, Nakagomi Y, Niwa H, Sang C, Kobayashi Y, Doyu M, Sobue G (2002) Testosterone reduction prevents phenotypic expression in a transgenic mouse model of spinal and bulbar muscular atrophy. Neuron 35:843–854.

Katsuno M, Adachi H, Doyu M, Minamiyama M, Sang C, Kobayashi Y, Inukai A, Sobue G (2003) Leuprorelin rescues polyglutamine-dependent phenotypes in a transgenic mouse model of spinal and bulbar muscular atrophy. Nat Med 9:768–773.

Katsuno M, Sang C, Adachi H, Minamiyama M, Waza M, Tanaka F, Doyu M, Sobue G (2005) Pharmacological induction of heat-shock proteins alleviates polyglutamine-mediated motor neuron disease. Proc Natl Acad Sci USA 102:16801–16806.

Katsuno M, Adachi H, Waza M, Banno H, Suzuki K, Tanaka F, Doyu M, Sobue G (2006) Pathogenesis, animal models and therapeutics in spinal and bulbar muscular atrophy (SBMA). Exp Neurol 200:8–18.

Kennedy WR, Alter M, Sung JH (1968) Progressive proximal spinal and bulbar muscular atrophy of late onset. A sex-linked recessive trait. Neurology 18:671–680.

Kobayashi Y, Kume A, Li M, Doyu M, Hata M, Ohtsuka K, Sobue G (2000) Chaperones Hsp70 and Hsp40 suppress aggregate formation and apoptosis in cultured neuronal cells expressing truncated androgen receptor protein with expanded polyglutamine tract. J Biol Chem 275:8772–8778.

LaMonte BH, Wallace KE, Holloway BA, Shelly SS, Ascano J, Tokito M, Van Winkle T, Howland DS, Holzbaur EL (2002) Disruption of dynein/dynactin inhibits axonal transport in motor neurons causing late-onset progressive degeneration. Neuron 34:715–727.

La Spada AR, Wilson EM, Lubahn DB, Harding AE, Fischbeck KH (1991) Androgen receptor gene mutations in X-linked spinal and bulbar muscular atrophy. Nature 352:77–79.

Li JY, Jahn R, Dahlstrom A (1995) Rab3a, a small GTP-binding protein, undergoes fast anterograde transport but not retrograde transport in neurons. Eur J Cell Biol 67:297–307.

Li JY, Pfister KK, Brady ST, Dahlstrom A (2000) Cytoplasmic dynein conversion at a crush injury in rat peripheral axons. J Neurosci Res 61:151–161.

Mangiarini L, Sathasivam K, Seller M, Cozens B, Harper A, Hetherington C, Lawton M, Trottier Y, Lehrach H, Davies SW, Bates GP (1996) Exon 1 of the HD gene with an expanded CAG repeat is sufficient to cause a progressive neurological phenotype in transgenic mice. Cell 87:493–506.

McCampbell A, Taylor JP, Taye AA, Robitschek J, Li M, Walcott J, Merry D, Chai Y, Paulson H, Sobue G, Fischbeck KH (2000) CREB-binding protein sequestration by expanded polyglutamine. Hum Mol Genet 9:2197–2202.

Minamiyama M, Katsuno M, Adachi H, Waza M, Sang C, Kobayashi Y, Tanaka F, Doyu M, Inukai A, Sobue G (2004) Sodium butyrate ameliorates phenotypic expression in a transgenic mouse model of spinal and bulbar muscular atrophy. Hum Mol Genet 13:1183–1192.

Morfini G, Pigino G, Szebenyi G, You Y, Pollema S, Brady ST (2006) JNK mediates pathogenic effects of polyglutamine-expanded androgen receptor on fast axonal transport. Nat Neurosci 9:907–916.

Münch C, Rosenbohm A, Sperfeld AD, Uttner I, Reske S, Krause BJ, Sedlmeier R, Meyer T, Hanemann CO, Stumm G, Ludolph AC (2005) Heterozygous R1101K mutation of the DCTN1 gene in a family with ALS and FTD. Ann Neurol 58:777–780.

Niwa H, Yamamura K, Miyazaki J (1991) Efficient selection for high-expression transfectants with a novel eukaryotic vector. Gene 108:193–199.

Nucifora Jr FC, Sasaki M, Peters MF, Huang H, Cooper JK, Yamada M, Takahashi H, Tsuji S, Troncoso J, Dawson VL, Dawson TM, Ross CA (2001) Interference by huntingtin and atrophin-1 with cbp-mediated transcription leading to cellular toxicity. Science 291:2423–2428.

Piccioni F, Pinton P, Simeoni S, Pozzi P, Fascio U, Vismara G, Martini L, Rizzuto R, Poletti A (2002) Androgen receptor with elongated polyglutamine tract forms aggregates that alter axonal trafficking and mitochondrial distribution in motor neuronal processes. FASEB J 16:1418–1420.

Puls I, Jonnakuty C, LaMonte BH, Holzbaur EL, Tokito M, Mann E, Floeter MK, Bidus K, Drayna D, Oh SJ, Brown Jr RH, Ludlow CL, Fischbeck KH (2003) Mutant dynactin in motor neuron disease. Nat Genet 33:455–456.

Puls I, Oh SJ, Sumner CJ, Wallace KE, Floeter MK, Mann EA, Kennedy WR, Wendelschafer-Crabb G, Vortmeyer A, Powers R, Finnegan K, Holzbaur EL, Fischbeck KH, Ludlow CL (2005) Distal spinal and bulbar muscular atrophy caused by dynactin mutation. Ann Neurol 57:687–694.

Ravikumar B, Vacher C, Berger Z, Davies JE, Luo S, Oroz LG, Scaravilli F, Easton DF, Duden R, O'Kane CJ, Rubinsztein DC (2004) Inhibition of mTOR induces autophagy and reduces toxicity of polyglutamine expansions in fly and mouse models of Huntington disease. Nat Genet 36:585–595.

Ribchester RR, Thomson D, Wood NI, Hinks T, Gillingwater TH, Wishart TM, Court FA, Morton AJ (2004) Progressive abnormalities in skeletal muscle and neuromuscular junctions of transgenic mice expressing the Huntington's disease mutation. Eur J Neurosci 20:3092–3114.

Roy S, Coffee P, Smith G, Liem RK, Brady ST, Black MM (2000) Neurofilaments are transported rapidly but intermittently in axons: implications for slow axonal transport. J Neurosci 20:6849–6861.

Sagot Y, Rosse T, Vejsada R, Perrelet D, Kato AC (1998) Differential effects of neurotrophic factors on motoneuron retrograde labeling in a murine model of motoneuron disease. J Neurosci 18:1132–1141.

Schmidt BJ, Greenberg CR, Allingham-Hawkins DJ, Spriggs EL (2002) Expression of X-linked bulbospinal muscular atrophy (Kennedy disease) in two homozygous women. Neurology 59:770–772.

Shea TB (2000) Microtubule motors, phosphorylation and axonal transport of neurofilaments. J Neurocytol 29:873–887.

Sobue G, Hashizume Y, Mukai E, Hirayama M, Mitsuma T, Takahashi A (1989) X-linked recessive bulbospinal neuronopathy. A clinicopathological study. Brain 112:209–232.

Sobue G, Hashizume Y, Yasuda T, Mukai E, Kumagai T, Mitsuma T, Trojanowski JQ (1990) Phosphorylated high molecular weight neurofilament protein in lower motor neurons in amyotrophic lateral sclerosis and other neurodegenerative diseases involving ventral horn cells. Acta Neuropathol (Berl) 79:402–408.

Sopher BL, Thomas Jr PS, LaFevre-Bernt MA, Holm IE, Wilke SA, Ware CB, Jin LW, Libby RT, Ellerby LM, La Spada AR (2004) Androgen receptor YAC transgenic mice recapitulate SBMA motor neuronopathy and implicate VEGF164 in the motor neuron degeneration. Neuron 41:687–699.

Steffan JS, Bodai L, Pallos J, Poelman M, McCampbell A, Apostol BL, Kazant-

sev A, Schmidt E, Zhu YZ, Greenwald M, Kurokawa R, Housman DE, Jackson GR, Marsh JL, Thompson LM (2001) Histone deacetylase inhibitors arrest polyglutamine-dependent neurodegeneration in *Drosophila*. Nature 413:739–743.

Sugars KL, Rubinsztein DC (2003) Transcriptional abnormalities in Huntington disease. Trends Genet 19:233–238.

Szebenyi G, Morfini GA, Babcock A, Gould M, Selkoe K, Stenoien DL, Young M, Faber PW, MacDonald ME, McPhaul MJ, Brady ST (2003) Neuropathogenic forms of huntingtin and androgen receptor inhibit fast axonal transport. Neuron 40:41–52.

Vonsattel JP, Myers RH, Stevens TJ, Ferrante RJ, Bird ED, Richardson Jr EP (1985) Neuropathological classification of Huntington's disease. J Neuropathol Exp Neurol 44:559–577.

Walker FO, Young AB, Penney JB, Dovorini-Zis K, Shoulson I (1984) Benzodiazepine and GABA receptors in early Huntington's disease. Neurology 34:1237–1240.

Waza M, Adachi H, Katsuno M, Minamiyama M, Sang C, Tanaka F, Inukai A, Doyu M, Sobue G (2005) 17-AAG, an Hsp90 inhibitor, ameliorates polyglutamine-mediated motor neuron degeneration. Nat Med 11:1088–1095.

Yamamoto A, Lucas JJ, Hen R (2000) Reversal of neuropathology and motor dysfunction in a conditional model of Huntington's disease. Cell 101:57–66.

Zu T, Duvick LA, Kaytor MD, Berlinger MS, Zoghbi HY, Clark HB, Orr HT (2004) Recovery from polyglutamine-induced neurodegeneration in conditional SCA1 transgenic mice. J Neurosci 24:8853–8861.

THE JOURNAL OF BIOLOGICAL CHEMISTRY VOL. 281, NO. 33, pp. 23842–23851, August 18, 2006

Archaeal Proteasomes Effectively Degrade Aggregation-prone Proteins and Reduce Cellular Toxicities in Mammalian Cells*

Received for publication, February 9, 2006, and in revised form, May 25, 2006 Published, JBC Papers in Press, June 22, 2006, DOI 10.1074/jbc.M601274200

Shin-ichi Yamada, Jun-ichi Niwa, Shinsuke Ishigaki, Miho Takahashi, Takashi Ito, Jun Sone, Manabu Doyu, and Gen Sobue[1]

From the Department of Neurology, Nagoya University Graduate School of Medicine, 65 Tsurumai-cho, Showa-ku, Nagoya-city, Aichi 466-8550, Japan

The 20 S proteasome is a ubiquitous, barrel-shaped protease complex responsible for most of cellular proteolysis, and its reduced activity is thought to be associated with accumulations of aberrant or misfolded proteins, resulting in a number of neurodegenerative diseases, including amyotrophic lateral sclerosis, spinal and bulbar muscular atrophy, Parkinson disease, and Alzheimer disease. The 20 S proteasomes of archaebacteria (archaea) are structurally simple and proteolytically powerful and thought to be an evolutionary precursor to eukaryotic proteasomes. We successfully reproduced the archaeal proteasome in a functional state in mammalian cells, and here we show that the archaeal proteasome effectively accelerated species-specific degradation of mutant superoxide dismutase-1 and the mutant polyglutamine tract-extended androgen receptor, causative proteins of familial amyotrophic lateral sclerosis and spinal and bulbar muscular atrophy, respectively, and reduced the cellular toxicities of these mutant proteins. Further, we demonstrate that archaeal proteasome can also degrade other neurodegenerative disease-associated proteins such as α-synuclein and tau. Our study showed that archaeal proteasomes can degrade aggregation-prone proteins whose toxic gain of function causes neurodegradation and reduce protein cellular toxicity.

The 20 S proteasome is a ubiquitous, barrel-shaped protease complex responsible for most of cellular proteolysis (1) and is formed by four stacked seven-membered rings (2). The α-type subunits, which are proteolytically inactive (3), form the outer rings, and the β-type subunits, which contain the active site (4), form the inner rings of the complex (5). The 20 S proteasome of archaebacteria (archaea) consists of only one type of each of the α- and β-subunits and is thought to be the evolutionary ancestor of the eukaryotic proteasome (6), which is quite similar in architecture to that of archaea but is composed of seven different α- and seven different β-subunits (6). Archaea do not have the ubiquitin recognition system for protein degradation and are thought to have unidentified tags in its degradation pathway (7). Like eukaryotic cells, archaea also have a regulatory complex for the 20 S proteasome, known as proteasome-activating nucleotidase (PAN)[2] (8). PAN is an evolutionary precursor to the 19 S base in eukaryotic cells and thought to be necessary for efficient archaeal 20 S proteasomal protein degradation (8). However *in vitro*, the archaeal 20 S proteasome has been reported to rapidly degrade polyglutamine aggregates without the help of PAN (9). This PAN-independent degradation by the archaeal 20 S proteasome inspired us to introduce and test a novel proteolytic facility in mammalian cells. We have chosen the archaeal *Methanosarcina mazei* (Mm) 20 S proteasome, because its optimal growth temperature is around 37 °C, making it suitable to examine its proteasomal effects in mammalian cells.

The eukaryotic ubiquitin-proteasome system degrades aberrant or misfolded proteins that could otherwise form potentially toxic aggregates (10). These aggregate formations in cells are related to the pathogenesis of several common aging-related neurodegenerative diseases, including Parkinson disease (PD), amyotrophic lateral sclerosis (ALS), polyglutamine diseases (*e.g.* Huntington disease, some spinocerebellar ataxias, and spinal and bulbar muscular atrophy), and Alzheimer disease (AD), which are thought to be associated with the reduced activities of the proteasome (11–15). However, a critical cause of the accumulation of abnormal proteins remains unclear. Solving this common aspect of many neurodegenerative disorders would be a breakthrough in treating these diseases.

In the present study, we show that the Mm proteasome functions in mammalian cells to accelerate the degradation of the following aggregation-prone proteins: mutant superoxide dismutase-1 (SOD1), a causative protein of familial ALS; mutant androgen receptor (AR) with expanded polyglutamine tract, a causative protein of spinal and bulbar muscular atrophy; α-synuclein, an accumulated protein in PD; and tau, an accumulated protein in AD.

* This work was supported by a Center of Excellence grant from the Ministry of Education, Culture, Sports, Science, and Technology of Japan. The costs of publication of this article were defrayed in part by the payment of page charges. This article must therefore be hereby marked "*advertisement*" in accordance with 18 U.S.C. Section 1734 solely to indicate this fact.

[1] To whom correspondence should be addressed. Tel.: 81-52-744-2385; Fax: 81-52-744-2384; E-mail: sobueg@med.nagoya-u.ac.jp.

[2] The abbreviations used are: PAN, proteasome-activating nucleotidase; SOD1, superoxide dismutase-1; Mm, *M. mazei*; ALS, amyotrophic lateral sclerosis; AR, androgen receptor; PD, Parkinson disease; AD, Alzheimer disease; MTS, 3-(4,5-dimethylthiazol-2-yl)-5-(3-carboxymethoxyphenyl)-2-(4-sulfophenyl)-2H-tetrazolium; WT, wild type; NTA, nitrilotriacetic acid; GFP, green fluorescent protein.

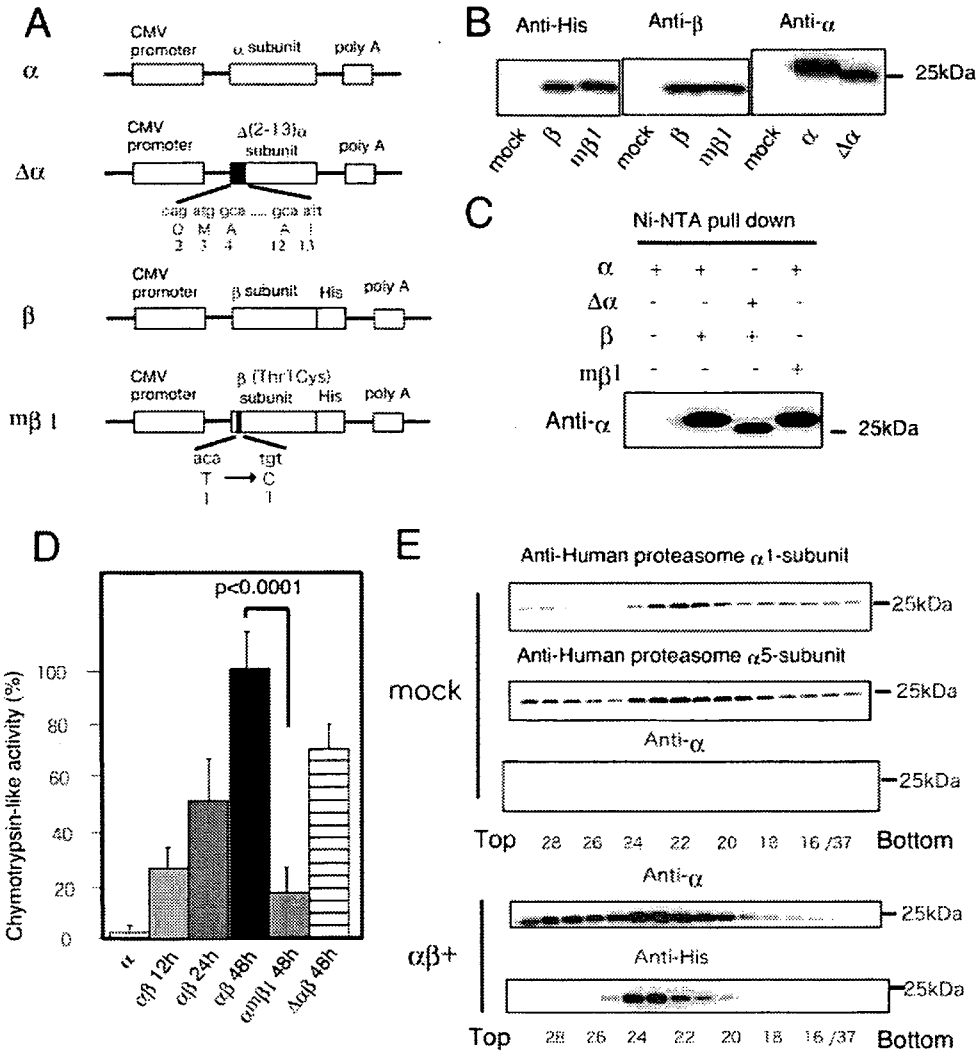

FIGURE 1. **Expression of *M. mazei* proteasome in mammalian cells.** *A*, schematic illustration of expression vectors used in this study. The deleted sequences of the Δα-subunit are depicted. The T1C β-subunit (mβ1) has three mutated base pairs (a to t, c to g, and a to t). *B*, Western blot analysis with anti-proteasome α-subunit, anti-proteasome β-subunit, and anti-His antibodies. *C*, Ni^{2+}-NTA pulldown assay. Pulled down proteins run on SDS-PAGE were probed with anti-proteasome α-subunit. *D*, chymotrypsin-like activity of the Ni^{2+}-NTA pulled down samples. This protease activity gradually became higher after transfection. *Error bars*, S.D. (n = 3). *E*, glycerol gradient centrifugation experiment: Mm proteasome α- and β-subunits fractionated into nearly the same fractions as did the human 20 S proteasome subunits α1 and α5, αβ− and αβ+, indicating that cells were transfected with mock and Mm proteasome αβ, respectively.

EXPERIMENTAL PROCEDURES

Construction of the Expression Vectors: M. mazei Proteasome Subunits α, β, ΔN(2–13)α, and Mutant β (T1C)—The DNA fragment encoding the α-subunit protein (GenBank™ accession number 1480962) was amplified by PCR from the genomic DNA of *M. mazei* (ATCC) using the following primers: αF (5′-GCGGGTACCCCACCATGCAGATGGCACCACAGATG) and αR (5′-CGCCTCGAGTTATTCTTTGTTCTCATTTCCTTTGTG). The Δ(2–13) α-subunit (Δα) was amplified using the following primers: ΔαF (5′-GCGGGTACCCCACCATGACGGTTTTCAGCCCTGACGG) and αR. The amplified fragments were inserted into the KpnI and XhoI site of the pcDNA 3.1(+) vector (Invitrogen). The β-subunit (GenBank™ accession number 1479036) was amplified by PCR with the following primers: βF (5′-GCCTCTAGACCACCATGGATAATGACAAATATTTAAAG) and βR (5′-GCGACCGGTGTTTCCTAAAGCTCTTCTG) and inserted into the XbaI and AgeI site of the pcDNA3.1(+)/MycHis vector (Invitrogen) to fuse it to a His_6 tag. The mutated mβ1-subunit (T1C β-subunit) was generated with a site-directed mutagenesis kit (Stratagene) following the manufacturer's protocol. Construction of pcDNA3.1/MycHis-SOD1 and pCMV-Tag4-SOD1 vectors (WT, G93A, G85R, H46R, and G37R) (16), pEGFP-N1-SOD1 (WT and G93A) vectors, pCR3.1-AR24Q and pCR3.1-AR97Q vectors, and pcDNA3.1(+)/MycHis-α-synuclein (WT, A53T, and A30P) was described previously (16–18). Six isoforms of tau were amplified by PCR from the pRK172 vectors that were kindly provided by Dr. Michel Goedert and inserted into the KpnI and XbaI site of the pcDNA3.1 vector (Invitrogen).

Cell Culture, Transfection, and Antibodies—Neuro2a cells and human embryonic kidney 293 (HEK293) cells were maintained in Dulbecco's modified Eagle's medium with 10% fetal calf serum. Transfections were performed using Lipofectamine 2000 (Invitrogen) in the 3-(4,5-dimethylthiazol-2-yl)-5-(3-carboxymethoxyphenyl)-2-(4-sulfophenyl)-2H-tetrazolium (MTS) assay or Effectene transfection reagent (Qiagen) in other experiments. Antibodies used here were as follows: anti-SOD1 antibody (SOD100; Stressgen Bioreagents), anti-His antibody (Ab-1; Oncogene), anti-α-tubulin antibody (clone B-5-1-1; Sigma), anti-20 S proteasome β-subunit antibody (from *Methanosarcina thermophila*; Calbiochem), anti-20 S proteasome α-subunit antibody (from *M. thermophila*; Calbiochem), anti-AR antibody (N-20; Santa Cruz Biotechnology, Inc., Santa Cruz, CA), anti-α-synuclein antibody (LB509; Zymed Laboratories Inc.), and anti-tau antibody (Mouse Tau-1; Chemicon International).

Glycerol Density Gradient Centrifugation—Cells grown on a 10-cm dish were lysed in 1 ml of 0.01 M Tris-EDTA, pH 7.5, by two freeze-thaw cycles, and the lysates were centrifuged for 15 min at 15 000 × *g* at 4 °C. The cleared supernatants were loaded on the top of a 36-ml linear gradient of glycerol (10–40%) prepared in 25 mM Tris-HCl buffer, pH 7.5, containing 1 mM dithiothreitol and then centrifuged at 80,000 × *g* for 22 h at 4 °C in a Beckman SW28 rotor (Beckman Coulter Inc.). Following centrifugation, 37 fractions (1.0 ml each) were collected from the top of the tubes with a liquid layer injector fractionator (model number CHD255AA; Advantech) connected to a fraction col-

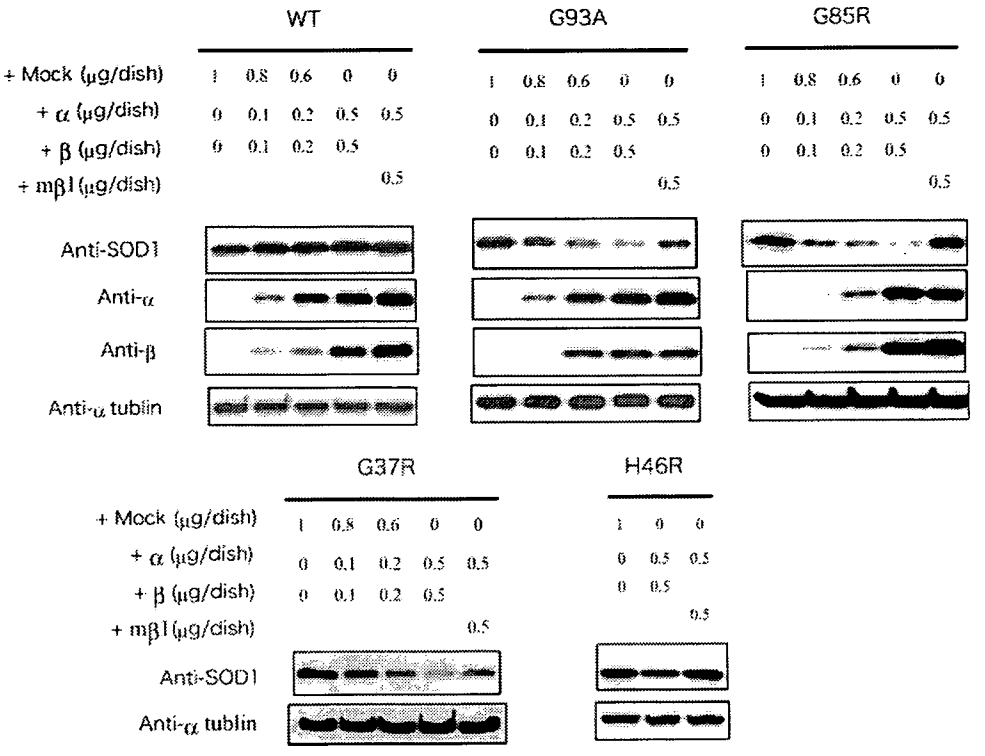

FIGURE 2. **Reduced expression levels of mutant SOD1 proteins in the presence of *M. mazei* proteasome.** Neuro2a cells grown on 6-cm dishes and co-transfected with 1 μg of SOD1-MycHis vector and increasing doses of Mm proteasome subunits were harvested and analyzed 48 h after transfection. The levels of mutant SOD1 proteins were gradually reduced as Mm proteasome αβ increased, whereas no changes in SOD1 proteins were seen with Mm proteasome αmβ1. *WT*, wild-type SOD1; *G93A*, $SOD1^{G93A}$; *G85R*, $SOD1^{G85R}$; *G37R*, $SOD1^{G37R}$; *H46R*, $SOD1^{H46R}$.

lector. 200 μl of each fraction was precipitated with acetone; the pellets were lysed with 50 μl of sample buffer and then used for SDS-PAGE followed by Western blotting. The immunostained bands were quantified using ImageGauge software (Fuji Film).

Ni^{2+}-NTA Pulldown—HEK 293 cells grown on 10-cm dishes, transfected with Mm proteasome α (as a control), αβ, Δαβ, and αmβ1, were lysed by two freeze-thaw cycles in 1 ml of phosphate-buffered saline buffer and centrifuged at 3000 × *g*. Proteasome complexes were pulled down from the supernatants with 200 μl of Ni^{2+}-NTA-agarose, washed 4 times in 4 ml of 10 mM imidazole/phosphate-buffered saline buffer, and eluted in 2 ml of 250 mM imidazole/phosphate-buffered saline buffer. Samples were then boiled and subjected to Western blotting.

Measurement of the Proteasome Activity—HEK 293 cells grown on 10-cm dishes were transfected with Mm proteasome α (as a control), αβ, Δαβ, and αmβ1. 12, 24, and 48 h after transfection, the cells were lysed and pulled down with Ni^{2+}-NTA. The chymotrypsin-like activity of 500 μl of the Ni^{2+}-NTA pulled down samples were assayed colorimetrically after 12-h incubations at 37 °C with 100 mM Suc-LLVY-amino-4-methylcoumarin (Sigma) by a multiple-plate reader (PowerscanHT, Dainippon Pharmaceutical). The assay was carried out in triplicate and statistically analyzed by one-way analysis of variance.

Immunocytochemistry—Neuro2a cells grown on glass coverslips were co-transfected with pEGFP-N1-SOD1 and Mm proteasome α- and His-tagged β-subunit. 48 h after transfection, cells were fixed, blocked, and incubated with anti-His antibody overnight at 4 °C. After washing, samples were incubated with Alexa-546-conjugated anti-mouse antibody (Molecular Probes, Inc.) and visualized with an Olympus BX51 epifluorescence microscope.

Cycloheximide Chase Analysis—Neuro2a cells grown on 6-cm dishes were transfected with 1 μg of pcDNA3.1/MycHis-SOD1 with mock (0.6 μg), Mm proteasome αmβ1 (0.3 μg each), or Mm proteasome αβ (0.3 μg each). 24 h after transfection, cycloheximide (50 μg/ml) was added to the culture medium, and the cells were harvested at the indicated time points. The samples were subjected to SDS-PAGE and analyzed by Western blotting with anti-SOD1 antibody.

Pulse-chase Analysis—Neuro2a cells grown on 6-cm dishes were transfected with 1 μg of pCMV-Tag4-$SOD1^{G93A}$ with mock (0.6 μg) Mm proteasome αmβ1 (0.3 μg each) or Mm proteasome αβ (0.3 μg each). 24 h after transfection, cells were pulse-labeled with [^{35}S]Cys for 60 min and harvested at the indicated time points. After the immunoprecipitation by anti-FLAG antibody (M2; Sigma), the samples were subjected to SDS-PAGE, phosphor-imaged (Typhoon 9410; Genaral Electric Co.), and statistically analyzed by one-way analysis of variance.

Cell Viability Analysis—HEK293 cells were grown on collagen-coated 96-well plates and co-transfected with pcDNA3.1/MycHis-SOD1 (WT, G93A, and G85R) and Mm 20 S proteasome αβ, αmβ1, or mock in 12 wells each. The MTS-based cell proliferation assays were performed after 48 h of transfection. Absorbance at 490 nm was measured at 37 °C in a multiple-plate reader (PowerscanHT, Dainippon Pharmaceutical). The assay was carried out in triplicate and statistically analyzed by one-way analysis of variance.

Caspase-3/7 Assay—HEK293 cells were grown on black 96-well plates and co-transfected with pcDNA3.1/MycHis-SOD1 (WT, G93A, and G85R) and Mm 20 S proteasome αβ, αmβ1, or mock. 24 h after transfection, the medium was replaced with serum-free medium (Dulbecco's modified Eagle's medium). After 24 h, activated caspase-3/7 activity was analyzed by the Apo-ONE homogeneous caspase-3/7 assay (Promega) following the manufacturer's instructions.

RESULTS

Cloning and Expression of M. mazei Proteasome—We cloned the Mm proteasome α-subunit (GenBank™ accession number 1480962) and β-subunit (GenBank™ accession number 1479036) from genomic DNA of Mm (Fig. 1*A*) and generated a mutant α-subunit lacking amino acids 2–13, Δ(2–13) α-subunit (Δα) (Fig. 1*A*). These amino acids (positions 2–13) nor-

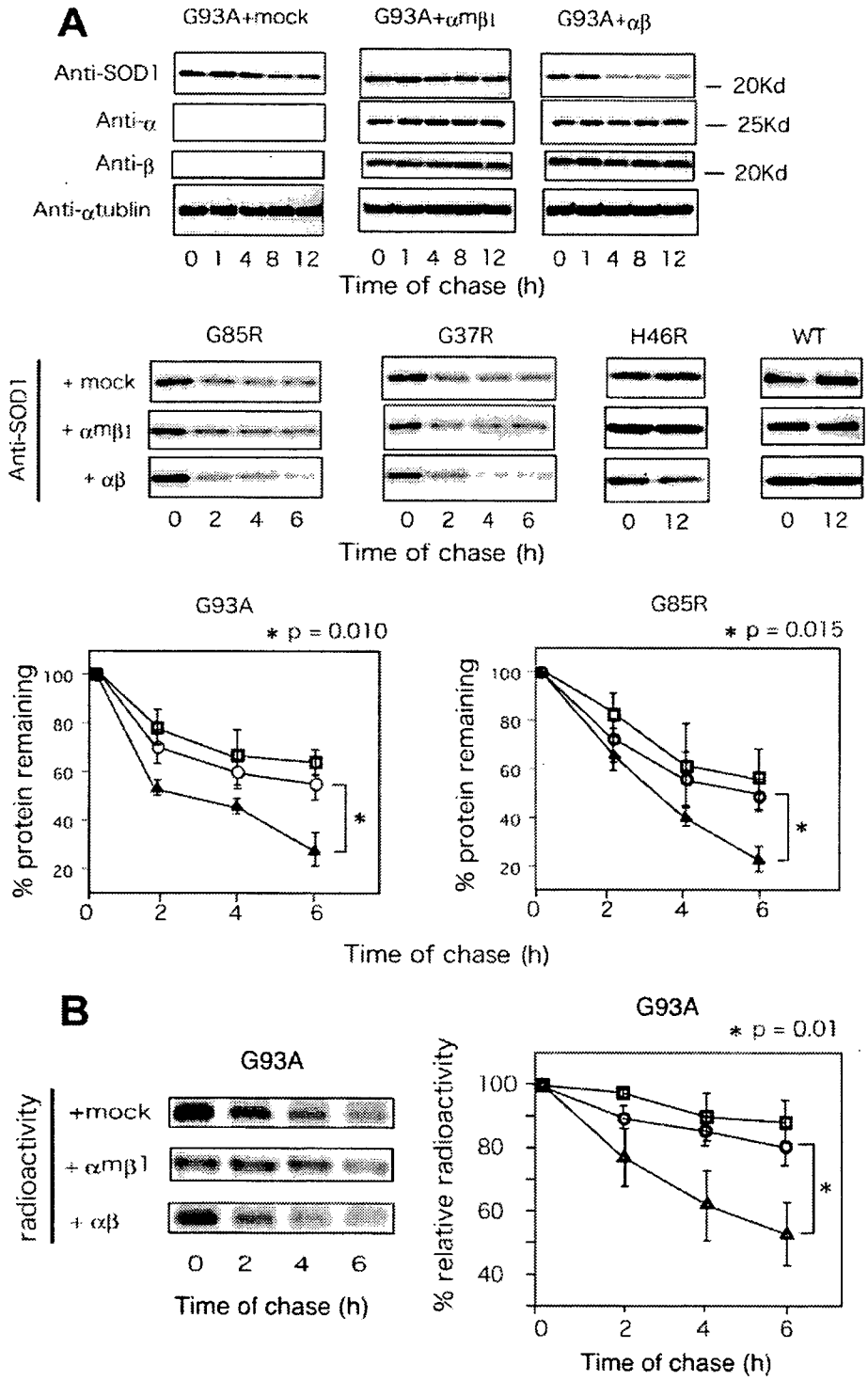

FIGURE 3. ***M. mazei* proteasome-accelerated degradation of mutant SOD1 proteins.** *A*, cycloheximide chase analysis (see "Experimental Procedures") showing that the half-lives of various mutant SOD1 proteins were reduced in the presence of Mm 20 S proteasome $\alpha\beta$. The *graphs* represent the percentage of degraded $SOD1^{G93A}$ and $SOD1^{G85R}$ proteins in three independent experiments. The *error bars* indicate S.D. *B*, pulse-chase analysis (see "Experimental Procedures") showing that the degradation of $SOD1^{G93A}$ was accelerated in the presence of Mm 20 S proteasome $\alpha\beta$. *Circle*, mock; *triangle*, $\alpha\beta$; *square*, $\alpha m\beta 1$. *Error bars*, S.D. ($n = 3$).

mally form a gated channel in the α-ring that regulates substrate entry into the 20 S proteasome (19). We also generated a mutant β-subunit with T1C ($m\beta 1$) (Fig. 1*A*). Thr-1 in the β-subunit of the archaeal proteasome is essential for proteolysis, and Thr-1 mutants lose their proteolytic activities (20). The following experiments were performed in both HEK293 and Neuro2a cells with similar results in both cell lines.

To confirm protein expression of the Mm subunits, HEK293 cells transfected with mock, α, $\Delta\alpha$, β, or $m\beta 1$ were lysed, subjected to SDS-PAGE, and immunoblotted with anti-proteasome α-subunit, anti-proteasome β-subunit, and anti-His antibodies. Fig. 1*B* demonstrates that the α- and β-subunit antibodies detected the Mm proteasome α-subunit at 26 kDa, the $\Delta\alpha$-subunit around 25 kDa, and the β-subunit at 22 kDa, respectively, and faintly recognized endogenous human proteasome subunits. A Ni^{2+}-NTA pull-down assay showed that the Mm proteasome α- and $\Delta\alpha$-subunits co-sedimented with the Mm proteasome β- and $m\beta 1$-subunits but not with mock (Fig. 1*C*), and protease activity of the pulled down samples of the cells lysed 48 h after transfection showed significantly higher chymotrypsin-like protease activity in the Mm proteasome $\alpha\beta$ than in the $\alpha m\beta 1$ or mock-transfected samples (Fig. 1*D*). This protease activity was confirmed to become gradually higher after transfection (Fig. 1*D*).

Glycerol density gradient centrifugation fractionated the $\alpha\beta$, $\Delta\alpha\beta$, and $\alpha m\beta 1$ complexes of the Mm proteasome into nearly the same fractions as those of the human 20 S proteasome subunits $\alpha 1$ and $\alpha 5$ (Fig. 1*E*, data not shown for $\Delta\alpha\beta$ and $\alpha m\beta 1$). Moreover, of the anti-His-immunoblotted bands (Fig. 1*E*), the density of staining in fractions 20–25 accounts for about 80–90% of the total anti-His staining. That these fractions constitute the majority of the anti-α staining as well suggests that about 80–90% of the β-subunit expression is incorporated into the Mm proteasome. These results suggested that the Mm proteasome α-, $\Delta\alpha$-, β-, and $m\beta 1$-subunits could properly assemble to form four stacked seven-membered rings and that an active Mm proteasome could be reproduced in mammalian cells. The cells expressing Mm proteasome $\Delta\alpha\beta$ displayed cellular toxicity, whereas the cells expressing Mm proteasome $\alpha\beta$ showed little toxicity

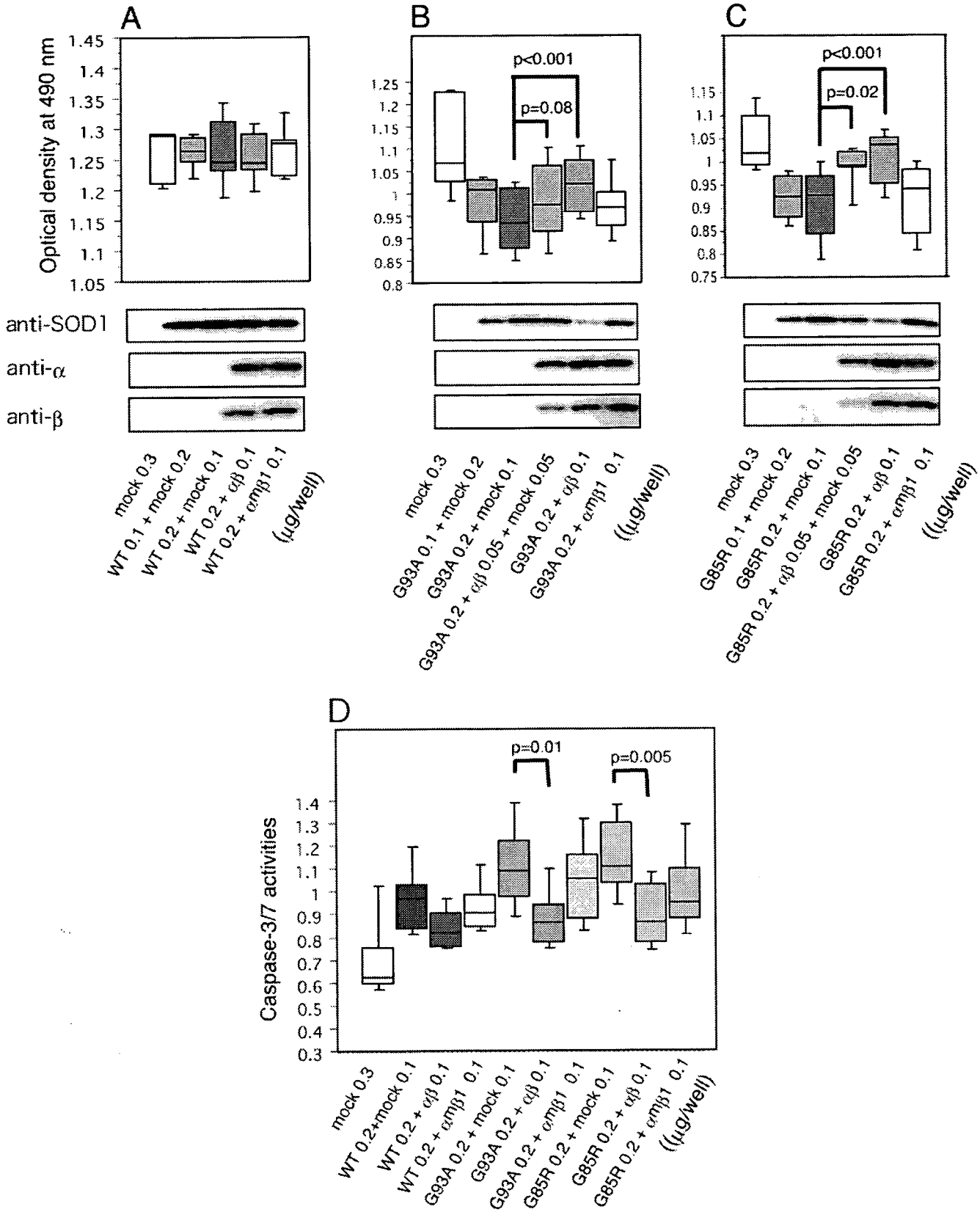

FIGURE 4. ***M. mazei* proteasome reduces the cellular toxicity of mutant SOD1.** The dose-dependent rescue effect of Mm proteasome $\alpha\beta$ expression on cell viability in $SOD1^{WT}$- (*A*), $SOD1^{G93A}$- (*B*), and $SOD1^{G85R}$-transfected HEK293 cells (*C*) as shown in MTS-based cell proliferation assays. The *box plots* show the median values (*center line* of *box*), the 25th (*lower line* of *box*), 75th (*upper line* of *box*), 10th (*lower T bar*), and 90th (*upper T bar*) percentiles in each group (n = 3 × 6 wells). The *numbers* indicate the dose of DNA transfected in each well of a 96-well plate ($\alpha\beta$, 0.1 μg; α, 0.05 μg; β, 0.05 μg). The expression levels of SOD1, α-subunit, and β-subunit at the analyzed points are shown. *D*, relative activities of cleaved caspase-3/7 were analyzed with the fluorescent caspase substrate, benzyloxycarbonyl-DEVD-R110. Production of Mm proteasome $\alpha\beta$ prevents activation of caspase-3/7. Positive control value was 3.2 ± 0.2 (S.D.) (n = 3 × 4 wells) (1 μM staurosporin, 24 h).

(data not shown); thus, further experiments were carried out with Mm proteasomes $\alpha\beta$ and $\alpha m\beta 1$.

M. mazei Proteasome Degrades Specifically Mutant Superoxide Dismutase-1—We then assessed whether the Mm proteasome actually affects mutant SOD1 protein ($SOD1^{G85R}$, $SOD1^{G37R}$, $SOD1^{G93A}$, and $SOD1^{H46R}$) expression. In cultured cells, mutant $SOD1^{G85R}$, $SOD1^{G37R}$, and $SOD1^{G93A}$ are more likely to form aggregates than is $SOD1^{H46R}$ (16), and cases of familial ALS expressing these mutant forms are also more severe than those expressing $SOD1^{H46R}$. Western blot analyses demonstrated that the levels of mutant SOD1 were markedly reduced as the expression of Mm proteasome $\alpha\beta$ increased (Fig. 2). However, wild-type SOD1 levels were not affected by the expression of Mm proteasome $\alpha\beta$. Furthermore, mutant SOD1 levels were not affected by the expression of Mm proteasome containing the $m\beta 1$-subunit in all mutant species, indicating that Mm proteasomal activity was important to reduce the levels of mutant SOD1 proteins. That the expression level of $SOD1^{H46R}$ was less affected by Mm proteasomal expression than other mutant SOD1 species may be associated with the lower toxicity of $SOD1^{H46R}$.

To determine whether the reduced levels of mutant SOD1 protein were due to accelerated degradation of mutant SOD1 or to the reduction of mutant SOD1 expression, we examined the stability of mutant SOD1 proteins expressed in Neuro2a cells co-expressed with Mm proteasome $\alpha\beta$, $\alpha m\beta 1$, or mock (Fig. 3, *A* and *B*). Chase experiments with cycloheximide, which halts all cellular protein synthesis, demonstrated mutant species-dependent acceleration in SOD1 protein degradation, whereas the expression levels of Mm proteasome α- and β-subunits did not change (Fig. 3*A*). The degree of wild-type SOD1 degradation was not affected by the expression of Mm proteasome $\alpha\beta$. Pulse-chase experiments further confirmed that ^{35}S-labeled $SOD1^{G93A}$ degradation was significantly accelerated when co-expressed with Mm proteasome $\alpha\beta$ but not with Mm proteasome $\alpha m\beta 1$ or mock (Fig. 3*B*). These facts strongly suggest that the catalytic center in the Mm proteasome β-subunit is important to accelerate the degradation of mutant SOD1 proteins.

M. mazei Proteasome Reduces Cellular Toxicities of Mutant Superoxide Dismutase-1—Next, we investigated the viability of HEK293 cells evoked by SOD1 (wild-type, $SOD1^{G93A}$, and $SOD1^{G85R}$) when co-expressed with Mm proteasome $\alpha\beta$, $\alpha m\beta 1$, or mock by the MTS-based cell proliferation assay (Fig. 4). We confirmed a linear response between cell number and optical density at 490 nm between 0.85 and 1.30 (data not shown). The viability of cells expressing wild-type SOD1 with Mm proteasome $\alpha\beta$ did not change as the transfected DNA doses of SOD1 and Mm proteasome $\alpha\beta$ increased (Fig. 4*A*). However, the viability of cells expressing mutant SOD1 was reduced as the transfected DNA dose of SOD1 increased (Fig. 4, *B* and *C*), and this reduction was prevented by the co-transfection with Mm proteasome $\alpha\beta$ but not with Mm proteasome $\alpha m\beta 1$. Toxicities of mutant SOD1 proteins are associated with the activation of caspase family proteins, especially caspase-3 (21). Using fluorescent substrates of activated caspase-3/7 as markers, we analyzed caspase-3/7 activities in the cells co-transfected with SOD1 proteins and with mock, Mm proteasome $\alpha\beta$, and $\alpha m\beta 1$. Mm proteasome $\alpha\beta$ suppressed the activation of caspase-3/7, resulting in reductions of cellular toxicities of SOD1 proteins (Fig. 4*D*). These results show that Mm proteasome $\alpha\beta$ has a protective effect against the decrease in cellular viability evoked by mutant SOD1.

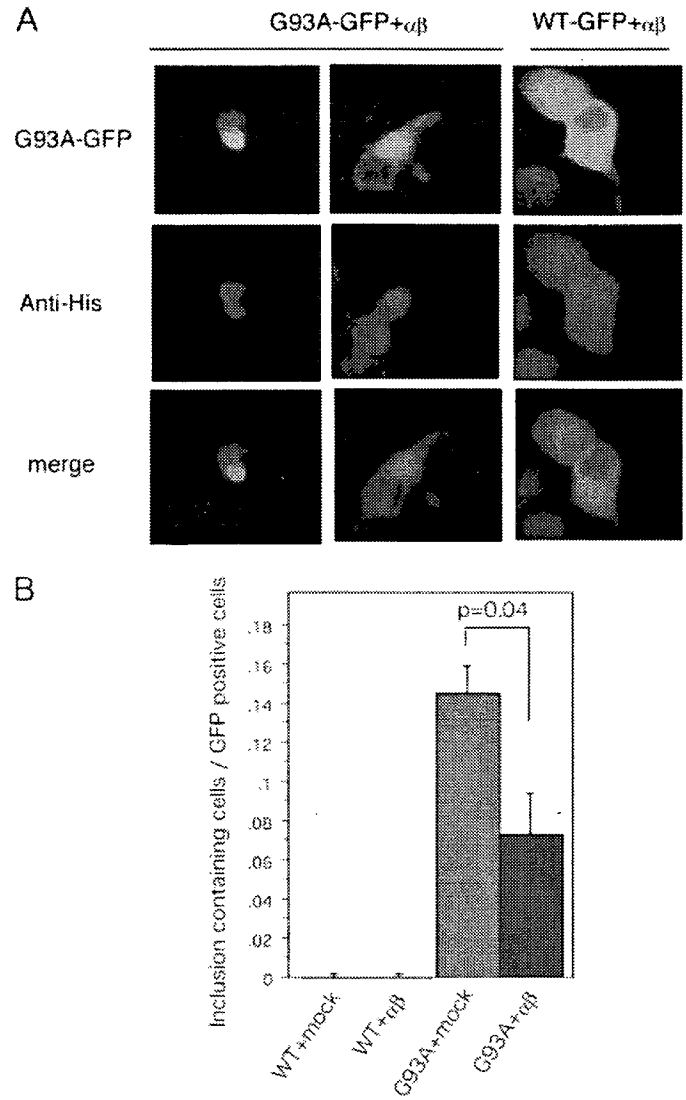

FIGURE 5. **Co-localization of mutant SOD1 and *M. mazei* proteasomes.** *A*, Neuro2a cells grown on glass coverslips were co-transfected with $SOD1^{WT}$-GFP or $SOD1^{G93A}$-GFP and Mm proteasome α- and His-tagged β-subunit. 48 h after transfection, cells were fixed, blocked, and incubated with anti-His antibody for 24 h. After washing, samples were incubated with Alexa-546-conjugated anti-mouse antibody. $SOD1^{G93A}$ and the Mm proteasome co-localized and formed aggregates together. *WT*, wild-type SOD1; *G93A*, $SOD1^{G93A}$. *B*, the percentages of aggregate-positive cells among the GFP-positive cells were determined. $SOD1^{G93A}$ aggregates were significantly reduced when co-expressed with Mm proteasome $\alpha\beta$. *Error bars*, S.D. (n = 3). Statistical analyses were carried out by Mann-Whitney's *U* test.

M. mazei Proteasome Co-localizes with Aggregates Formed by Mutant SOD1—In the assembly process of the archaeal proteasome, α-subunit assembly is required for β-subunit incorporation into the proteasome (20), and since the anti-His-stained β-subunit is restricted largely to that incorporated into the Mm proteasome (Fig. 1*E*), we used anti-His staining to localize the transfected proteasome in Neuro2a cells. GFP-tagged wild-type and G93A mutant SOD1 vectors were transfected along with Mm proteasome $\alpha\beta$ into Neuro2a cells, which were then fixed and immunostained with anti-His antibody. Fig. 5*A* shows that